Distribution of paramagnetic and diamagnetic cortical substrates following mild Traumatic Brain Injury: A depth- and curvature-based quantitative susceptibility mapping study

Christi A. Essex[1,*] **Jenna L. Merenstein**[2] **Devon K. Overson**[2] **Trong-Kha Truong**[2] **David J. Madden**[2] **Mayan J. Bedggood**[1] **Helen Murray**[3] **Samantha J. Holdsworth**[4] **Ashley W. Stewart**[5] **Catherine Morgan**[6] **Richard L. M. Faull**[3] **Patria Hume**[7] **Alice Theadom**[1] **Mangor Pedersen**[1]

[1]Department of Psychology and Neuroscience, Auckland University of Technology, Auckland 0627, New Zealand
[2]Brain Imaging and Analysis Center, Duke University Medical Center, Durham, NC 27710, United States
[3]Center for Brain Research, The University of Auckland, Auckland 1023, New Zealand
[4]Mātai Medical Research Institute, Gisborne 4010, New Zealand
[5]Center for Advanced Imaging, The University of Queensland, Queensland 4067, Australia
[6]Center for Advanced MRI, The University of Auckland, Auckland 1023, New Zealand
[7]Sports Performance Research Institute New Zealand, Auckland University of Technology, Auckland 0627, New Zealand
[*]Corresponding author: Department of Psychology and Neuroscience, Auckland University of Technology, Auckland 0627, New Zealand. Email: christi.essex@autuni.ac.nz

ABSTRACT

Evidence has linked head trauma to increased risk factors for neuropathology, including acute mechanical deformation of the cortical sulcal fundus and, later, perivascular accumulation of hyperphosphorylated tau (p-tau) adjacent to these spaces related to chronic traumatic encephalopathy (CTE). Despite this, little is known about microstructural abnormalities and cellular dyshomeostasis at the acute stage of mild traumatic brain injury (mTBI) in humans, particularly in the cortex. To address this gap in the literature, we designed the first architectonically-motivated quantitative susceptibility mapping (QSM) study to assess regional patterns of positive (iron-related) and negative (myelin-, calcium-, and protein-related) magnetic susceptibility in cortical regions of interest (ROI) following mTBI. Depth- and curvature-specific positive and negative QSM values were compared between 25 males with acute (< 14 days) sports-related mTBI (sr-mTBI) and 25 age-matched male controls across 34 cortical ROIs. Bilateral between-group analyses were conducted on specific ROI curvature bins (crown, bank, and fundus) as well as a combined curvature measure, across 21 cortical depths, for each ROI. Correlations between positive and negative susceptibility were analysed for age, brain injury severity, and the number of days since injury. We observed significant group differences in magnetic susceptibility for depth, curvature, and ROIs. Our results suggest a trauma-induced pattern of likely iron deposition preferential to superficial, perivascular-adjacent spaces in the sulci of the parahippocampal gyrus. Co-localised decreases in diamagnetism in the same region suggest dual pathology of neural substrates, the biological mechanisms behind which remain speculative. Significant correlations were found between magnetic susceptibility and age, both in ROIs and cortical depths distinct from those showing sr-mTBI-related differences. Little to no relationship was observed between magnetic susceptibility and subjective markers of injury or injury latency. The coherence between our findings and pathognomonic patterns of misfolded proteins in trauma-related neurodegeneration is interesting, which may have implications for the role of brain iron in microstructural cortical tissue damage after a mild brain injury. Further longitudinal research is needed to elucidate the long-term implications of our findings.

INTRODUCTION

Mild traumatic brain injury (mTBI) is responsible for up to 90% of the estimated 27-69 million annual incidents of traumatic brain injury worldwide;[1–3] representing a ∼USD $400 billion global economic burden.[4] In addition to economic impacts, exposure to mild head trauma is a major public health concern. mTBI is associated with adverse mental health effects, cognitive decline, increased risk of neurodegenerative disease,[5,6] and premature mortality.[7] Repeated instances of brain trauma is a well documented risk factor for the progressive tauopathy known as chronic traumatic encephalopathy (CTE), most often observed in athletes as a result of participation in contact sports, or in military veterans from exposure to blast impacts.[8–14] mTBI is characterised by a primary insult to the brain, affecting tissue microstructure and inducing a cascade of secondary cellular processes, transient states of metabolic distress, and cellular dyshomeostasis.[15] The absence of discernible focal lesions or other macroscopic morphological abnormalities means standard neuroimaging approaches are often insufficiently sensitive to detect mTBI pathology.[16,17] Advanced

neuroimaging methods extending beyond the scope of conventional medical practices may be used to identify the subtle, diffuse, and heterogeneous changes in brain structure.[18,19] Despite promising advances toward discovery of mTBI biomarkers, to date no specific markers of structural brain injury have been identified and assessments are thus restricted to clinical evaluations and self-reported impairments in cognitive and physiological function.[17,20] These assessments may not accurately reflect objective measures of brain injury or recovery status, which can constrain intervention efficacy.[20,21]

Investigating the role of biomaterials involved in preserving neuronal homeostasis, including trace elements such as brain iron, represents a promising direction for biomarker research. Iron is essential for proper brain function, and is a cofactor in various neuronal processes including neurotransmitter-, myelin-, and DNA-synthesis, energy metabolism, and oxidative phosphorylation.[22] Cellular concentrations are tightly regulated within neural tissue and dyshomeostasis has been linked to oxidative stress, DNA and protein damage, inflammation, and ferroptosis (a form of iron-regulated cell death).[23–25] Evidence suggests iron overload is implicated in both secondary injury and the emergence of pathology downstream[26] including hyperphosphorylation of tau (p-tau),[27] highlighting the direct interplay between elevated levels of iron and CTE-like processes. Histologically-validated co-localisation of iron with abnormal protein accumulations in progressive tauopathies has distinguished brain iron as a hallmark feature of degenerative disorders such as Alzheimer's and Parkinson's disease (AD and PD, respectively)[28,29] and has been cited within neurofibrillary tangles in CTE.[30] Despite evidence linking head trauma to increased risk factors for premature iron-related neuropathology[31] and increased levels of brain iron in humans following mTBI,[25] the association between brain iron accumulation and the pathophysiology of acute sports-related mild traumatic brain injury (sr-mTBI) remains unclear.

Quantitative susceptibility mapping (QSM), an advanced magnetic resonance imaging (MRI) method, measures intrinsic magnetic properties and spatial distributions of biomaterials and molecules (including iron, calcium, protein, and myelin) that are related to brain tissue composition.[32–37] The magnetic susceptibility of these materials is proportional to the degree of magnetisation exhibited in response to an external magnetic field, such as the main magnetic field of an MRI scanner (B_0).[38] Differences in magnetic field perturbation from dia- and para-magnetic compounds in brain tissue create inhomogeneities in the phase maps of gradient-recalled echo (GRE) MRI sequences.[39–41] This mechanism generates contrast in QSM, thereby providing insights into the architecture of the brain and enabling more accurate delineation of many structural boundaries than the corresponding GRE magnitude images.[42] Unlike traditional susceptibility-weighted imaging (SWI) from which QSM is derived, this approach can be used to directly quantify the susceptibility of tissue within regions of interest (ROIs), serving as a close approximation of the constituent elements.[43,44] Already integral to dementia research,[45–50] QSM can be extended to investigate potential susceptibility-related pathology resulting from acute sr-mTBI.

A limited number of studies have used QSM to quantify magnetic susceptibility in white matter and/or subcortical or global grey matter,[51–57] or as a marker of cerebral venous oxygen saturation ($Sv0_2$).[56,58,59] QSM investigations of mTBI-related grey matter alterations have focussed almost exclusively on deep grey nuclei as a proxy for injury effects and cellular degeneration. This is due to the high density of iron in these nuclei related to elevated metabolic demand,[26] particularly in the globus pallidus, red nucleus, substantia nigra, putamen, dentate, caudate, and thalamus, relative to the cortical grey matter.[60] These deep grey matter sites are not only vulnerable to iron-mediated disorders[61] but also damage in mTBI.[62] However, studies using QSM to investigate mTBI effects have largely overlooked the cortex. This complex structure is characterised by ridges (gyri) and grooves (sulci); curvatures corresponding to the base (fundus) of these sulci are exposed to the greatest force during mTBI, a phenomenon referred to as the 'water hammer effect.'[63]

These cortical, microvascular-adjacent, regions most susceptible to mechanical deformation and injury in mTBI are also the primary loci of degeneration and tauopathy in CTE[12,64] and warrant careful investigation. The singular mTBI-QSM study to include cortical grey matter ROIs[52] was constrained by a macroscopic voxel-wise approach. Significantly more anatomical precision is needed to detect depth- or curvature-specific differences in magnetic susceptibility within the cortical mantle after mTBI. The cortex is likely excluded from investigation due to several methodological challenges primarily related to complex cortical architectonics. Firstly, differentiating myeloarchitecture, cytoarchitecture, and cortical laminae using ultra-high field, ultra-high resolution MRI (such as that acquired at 7T or higher), is a developing area in neuroimaging research.[65] Currently, however, most research institutions pri-

marily use MRI scanners with lower field strengths. Secondly, standard voxel-wise comparisons are naïve to the architectonics and distribution of cellular elements within the cortical layers; here, advanced analytic techniques are essential. At magnetic field strengths of 3T or lower, and supra-millimetre voxel resolutions, analysis of specific cortical laminae is inhibited; however, column-based analytic techniques [66–69] enable depth-wise investigations of magnetic susceptibility in the cerebral cortex and are already producing promising results in Alzheimer's research. [67]

To address these research gaps, we conducted the first architectonically-motivated QSM analysis of cerebral mTBI effects. This study aimed to: 1) assess regional patterns of positive (iron-related) and negative (myelin-, protein-, calcium-related) magnetic susceptibility as a marker of acute cortical pathology after sr-mTBI, and; 2) understand the relationship between magnetic susceptibility in the cerebral cortex and variables such as age, injury latency, and severity. Based on prior literature, we hypothesised that differences in susceptibility would likely be evident in the frontal and temporal cortices, which are reported to be susceptible to injury in mTBI and are among the first to show degenerative effects of brain injury. We expected this distribution to be most prominent in the sulcal fundus due to increased vulnerability to trauma-induced deformation. Based on known effects of age on cortical iron deposition in this age range, [60] positive susceptibility values were hypothesised to show a positive relationship with age; however, correlation analyses remained largely exploratory and without specific *a priori* hypotheses.

MATERIALS AND METHODS

Approval for this study was granted by both The Auckland University of Technology Ethics Committee ((AUTEC) Date: 18/02/2022, Ref: 22/12) and the Health and Disabilities Ethics Committee ((HDEC) Date: 18/02/2022, Ref: 2022 EXP 11078). The study was conducted following the Declaration of Helsinki and all participants provided written informed consent prior to data collection. All participants were provisioned a $50NZD food voucher to acknowledge their contribution as well as a $20NZD fuel voucher or taxi chit to cover travel expenses related to MRI scan attendance.

Participants

Data from 25 male contact sports players (M = 21.10 years old [16-32], SD = 4.43) with acute sr-mTBI (< 14 days; M = 10.40 days, SD = 3.03) and 25 age-matched male controls (M = 21.10 years old [16-32], SD = 4.35) were used for this observational, case-control study (see Table 1). Clinical (sr-mTBI) participants were recruited through three Axis Sports Medicine clinics (Auckland, New Zealand) and through community-based pathways including referrals from healthcare professionals and sports team management. All clinical participants received a confirmed diagnosis of sr-mTBI by a licensed physician as a prerequisite for study inclusion and symptom severity was assessed with the Brain Injury Screening Tool (BIST) [70] upon presentation to Axis clinics or electronically after recruitment. Healthy controls were recruited through print and social media advertisements, and word-of-mouth. A history of significant medical or neurological conditions unrelated to the scope of this study or contraindication for MRI precluded study participation. Additionally, controls were excluded if they: i) had any recent history of mTBI events (< 12 months); ii) were living with any long-term effects of previous mTBI, or; iii) had sustained more than 5 lifetime events of mTBI. All participants completed a 1 hour MRI scan and a short demographic questionnaire. All MRI testing was conducted at The Centre for Advanced MRI (CAMRI), Auckland, New Zealand and relevant scans were reviewed for clinically significant findings by a certified radiologist to ensure participant safety.

Table 1: Summary of sr-mTBI participant clinical characteristics with reference to healthy controls

ID	Age	DSI	BIST Score	MOI	MRI findings
mTBI-01	< 20	5 days	140	Rugby	None
mTBI-02	< 20	5 days	12	Rugby	None
mTBI-03	20s	6 days	78	Rugby	None
mTBI-04	< 20	13 days	18	Rugby	Small fluid signal spaces in R peritrigonal WM - normal. R caudate cleft along ventricular surface - possibly developmental or from old ischaemic insult. Not clinically relevant
mTBI-05	< 20	12 days	61	Rugby	None
mTBI-06	20s	13 days	42	Rugby	None
mTBI-07	20s	13 days	13	Football	Minor artifactual T1 signal in pons. Not clinically relevant
mTBI-08	20s	12 days	6	Hockey	None
mTBI-09	20s	6 days	56	Rugby	Minor R orbital fracture (old). Not clinically relevant
mTBI-10	< 20	12 days	54	Rugby	None
mTBI-11	20s	10 days	52	Rugby	None
mTBI-12	30s	13 days	13	Football	None
mTBI-13	< 20	5 days	79	Rugby	None
mTBI-14	20s	13 days	2	Rugby	Small focus of susceptibility in L superior frontal gyrus possibly vascular or nonspecific haemosiderin. Not clinically relevant
mTBI-15	< 20	13 days	22	Rugby	None
mTBI-16	< 20	8 days	117	Futsal	Tiny cleft of fluid signal in R cingulate gyrus - minor developmental anomaly or mature gliosis. Not clinically relevant
mTBI-17	20s	13 days	*	Rugby	None
mTBI-18	20s	10 days	34	Gymnastics	None
mTBI-19	20s	13 days	28	Jiu-jitsu	Some artifactual DWI signal in pons. Not clinically relevant
mTBI-20	20s	11 days	69	Surfing	Tiny susceptibility site in R temporal lobe - may be vascular. Not clinically relevant
mTBI-21	< 20	7 days	14	Rugby	Minor susceptibility in transverse sulcus in R mid temporal lobe - nonspecific, may be vascular or reflect haemosiderin deposition from prior small volume haemorrhage. Not clinically relevant
mTBI-22	< 20	13 days	39	Judo	None
mTBI-23	< 20	9 days	34	Rugby	None
mTBI-24	< 20	12 days	68	Rugby	None
mTBI-25	20s	12 days	17	Rugby	7mm pineal cyst - normal limits. Some T1 hyperintensity in R cerebellum - artefact compatible. Not clinically relevant
Mean	21.10 (4.43) years	10.4 (3.03) days	44.5 (35.0) /160		No incidental findings. Non-incidental findings not considered clinically relevant
Mean HC	21.10 (4.35) years				No incidental findings. Non-incidental findings not considered clinically relevant

Note. Diagnostic assessment is limited to the volume T1, SWI and DWI sequences with only limited interpretation of the multi-echo T2 stack. Clinical assessments are relevant to identification of micro-haemorrhages, areas of siderosis, T1 appearance, gliosis, volume, ventricular volumes and non-neurological findings. Age is given in a range to prevent re-identification of participants. Possible range of BIST scores are 0 (min) to 160 (max). Clinical group data correspondent to date at MRI only with the exception of the BIST[70] acquired >24 hours post-injury prior to MRI scanning (<14 days post). Abbreviations are as follows: ID = unique identifier; DSI = days since injury; BIST = Brain Injury Screening Tool;[70] MOI = mechanism of injury; MRI = magnetic resonance imaging; L = Left; R = right; * = missing data.

Neuroimaging

Acquisition

Advanced MRI data were acquired on a 3T Siemens MAGNETOM Vida Fit scanner (Siemens Healthcare, Erlangen, Germany) equipped with a 20-channel head coil. A 3D flow-compensated GRE sequence was used to obtain magnitude and phase images for QSM reconstruction at 1 mm isotropic resolution (TR = 30 ms; TE = 20 ms; FA = 15°; slice thickness = 1.0 mm; FoV = 224 mm; matrix size = 180 x 224 x 160 mm) for a total acquisition time of ~ 3.43 minutes. For each participant, a high-resolution 3D T1-weighted (T1w) anatomical image volume was acquired for coregistration, parcellation and segmentation using a Magnetisation-Prepared Rapid Acquisition Gradient Echo (MPRAGE) sequence (TR = 1940.0 ms; TE = 2.49 ms, FA= 9°; slice thickness = 9 mm; FoV = 230 mm; matrix size = 192 x 512 x 512 mm; GRAPPA = 2; voxel size 0.45 x 0.45 x 0.90 mm) for a total acquisition time of ~ 4.31 minutes. T2 maps, resting-state functional MRI data, diffusion-weighted images, and susceptibility-weighted images were also acquired as part of a larger study and analysed separately. Participant DICOM images were converted to NIfTI files and transformed to brain imaging data structure (BIDS)[71] for further processing using *Dcm2Bids*[72] version 3.1.1, which is a wrapper for *dcm2niix*[73] (v1.0.20230411).

Anatomical image processing

First, bias field correction was performed on the T1w images for each subject using the *N4* algorithm[74] from ANTs.[75] The bias field-corrected T1w images were processed in FreeSurfer[76] to 1) delineate pial and grey matter/white matter (GM/WM) boundary meshes,

and; 2) generate estimates of cortical thickness and curvature for each vertex.[67] Skull-stripping was re-run with additional arguments, including *-gcut* and adjustments to the watershed threshold as needed, to improve the accuracy of the original FreeSurfer[76] pial surface mesh. The pipeline for T1w and QSM image processing is summarised in Figure 1.

QSM processing

QSM images were reconstructed using QSMxT[77] v6.4.2 (https://qsmxt.github.io/QSMxT/) available as a container via NeuroDesk[78] (v2024-03-27), a lightweight virtual environment. QSMxT integrates and automates phase unwrapping using a rapid open-source minimum spanning tree algorithm (ROMEO),[79] background field removal with projection onto dipole fields (PDF),[80] and sparsity-based rapid two-step dipole inversion (RTS);[81] a pipeline congruent with recent consensus statement recommendations for best-practice QSM reconstruction.[82] QSMxT also enables a novel two-pass combination method for hole-filling and artefact reduction[83] which performs parallel QSM masking and reconstruction on susceptibility sources identified as reliable and less reliable. Dual QSM images are then combined into a final integrated image more robust to reconstruction errors and streaking artefacts than those produced using a single-pass approach.[83] A brain mask was also generated using FSL's *BET*[84] to improve masking and hole-filling of the threshold-based selection algorithm[85] used for two-pass QSM.

Subsequent processing was performed locally using FSL.[86–88] For each subject, the raw magnitude image was skull-stripped using FSL's *BET*[84] with robust brain centre estimation and a fractional intensity threshold of between 0.3 and 0.6. Binary masks were derived from the skull-stripped magnitude image and applied to the susceptibility maps to erode non-brain noise around the brain perimeter using *fslmaths*. Skull-stripped T1-weighted images were used for the linear coregistration of the magnitude image using FMRIB's Linear Image Registration Tool (*FLIRT*)[89–91] with 12 degrees of freedom (DoF). Due to variability in acquisition parameters, FoV, and matrix size between subject images, the 12 DoF linear registration provided more accurate alignment compared to the 6 DoF alternative, allowing for better compensation of non-rigid anatomical variations upon visual inspection. The resulting transformation matrix was used for spatial normalisation of the QSM images to T1w space, effectively upsampling the QSM images. As the analyses are based on cortical depth rather than voxel-wise comparisons, upsampling was not considered a concern. In line with prior research,[67] QSM maps were then thresholded into separate sign (positive and negative) susceptibility maps with *fslmaths*. Traditional QSM maps represent average voxel-wise susceptibility distributions,[92] thereby obscuring individual susceptibility sources. Thresholding may enable better distinction of materials with varying biomagnetic properties (e.g., paramagnetic (likely iron) and diamagnetic (likely myelin, calcium, and protein)), and may facilitate a more precise estimation of neurobiological characteristics in analyses.

Cortical column generation

To generate cortical columns and sample signed susceptibility values, we used a pipeline previously applied to DWI data analysis[66] and recently adapted for use with QSM.[67] First, the T1w FreeSurfer[76] recon served as an input into the *easy_lausanne* tool (https://github.com/r
This stripped-down fork of the open-source Connectome Mapper[93] separates the cortex into five atlases, ranging from 34 to 250 ROIs per hemisphere, according to the Lausanne multi-scale atlas.[94] For subsequent analyses, we focused on the atlas with 34 ROIs per hemisphere, which is equivalent to the Desikan-Killiany atlas[95] native to FreeSurfer.[76]

Cortical columns were created for each hemisphere in T1w space with *write_mrtrix _tracks*[96] in MATLAB (version R2024a), which was used to connect vertex pairs between the pial and GM/WM boundary surface meshes. Each cortical column was segmented into 21 equidistant depths, each with a step size of 5% of the cortical thickness,[65,69] from the pial surface to the GM/WM boundary using MRtrix3 *tckresample*.[96] Here, the step-wise depths represent the 21 equidistant segmentations rather than specific cellular laminae (L1 to L6) of the cortex. It is important to distinguish results produced using this approach from ultra-high field investigations of cyto- and myelo-architecture in the cerebral cortex; results described herein are related to cortical *depth*, rather than *layer*. The columns were categorised based on cortical curvature, derived from FreeSurfers[76] Gaussian curvature values at each GM/WM boundary vertex[97] and quantified in units of $1/mm^2$. The categories included the gyral crown (curvature values: 0.6 to 0.1), sulcal bank (0.1 to 0.1), and sulcal fundus (0.1 to 0.6).[67] Positive curvature values indicated sulci, while negative values indicated gyri, with higher values corresponding to deeper curvatures.[67] Only columns ranging from 0.5 mm to 6 mm in length were included in the analysis to capture plausible cortical morphology.[98] Depth was measured in percentage of cortical thickness rather

than absolute metrics (mm) to mitigate any variability between control and clinical participants.

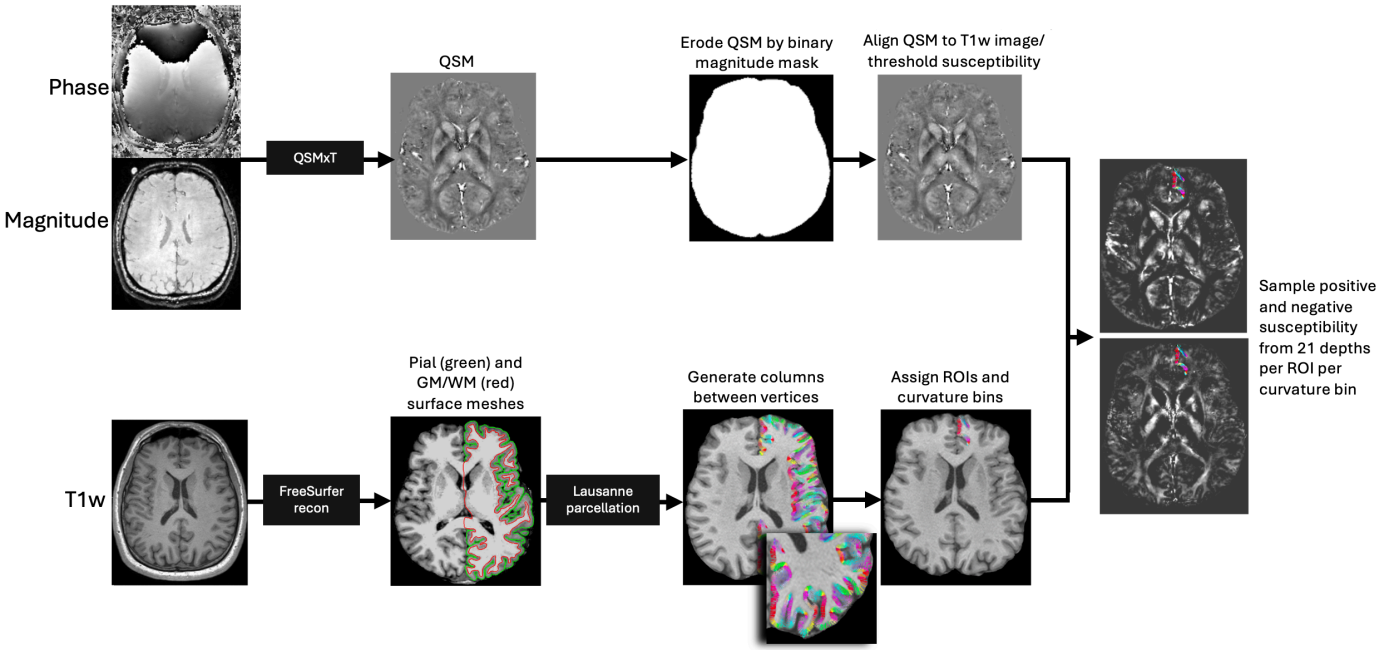

Figure 1: Image processing pipeline
Steps are performed independently and in parallel for each participant. Quantitative susceptibility maps were reconstructed from magnitude and phase images using QSMxT, and eroded by the skull-stripped, binarised magnitude image mask to remove non-brain sources of susceptibility. QSM images were then aligned to T1-weighted images, and thresholded into positive and negative susceptibility maps. FreeSurfer recon was used on bias field-corrected T1-weighted images to produce pial and GM/WM boundary surface meshes, and vertex pairs were then joined to create cortical columns. Parcellations of the cortical grey matter were estimated by feeding the T1w FreeSurfer recon into *easy_lausanne*. Columns were then assigned specific ROIs and curvature bins, and used to sample susceptibility from thresholded QSM maps.

Statistical analyses

To provide a detailed analysis of microstructural differences associated with sr-mTBI while maintaining result granularity, we performed analyses at the bilateral regional level using MATLAB (2024a). Average positive and negative susceptibility values were extracted from 21 cortical depths for all 34 ROIs. Each ROI was analysed by independent curvature bin (gyral crown, sulcal bank, and sulcal fundus) as well as combined curvature as a whole-ROI measure. To control for multiple comparisons and align with prior research,[67] we applied a false discovery rate (FDR) correction[99] to the p-values for 21 comparisons (one for each depth) for each ROI/curvature profile. Due to precise age-matching of participants, age was not considered a covariate or confounding variable of interest for between-group comparisons. However, to explore the relationship between QSM values and age in the entire sample, partial Pearson correlation coefficients were calculated between age and both positive and negative susceptibility values independently for all 34 curvature-combined ROIs, at each depth, whilst controlling for group effects. To explore the relationship between susceptibility values and other sr-mTBI-related variables, Pearson correlation coefficients were also calculated between Brain Injury Screening Tool (BIST)[70] scores and injury latency (days since injury (DSI)) and both positive and negative susceptibility values independently for the the sr-mTBI sample only. mTBI-17 was excluded from correlations between BIST and both susceptibility signs due to missing data. Correlations were also corrected for 21 depth-wise comparisons using FDR procedures.[99] Given the limited sample size and the need to conserve degrees of freedom in this exploratory study, regression analyses were deliberately omitted.

RESULTS

Regional depth- and curvature-based analyses

Using independent sample t-tests, we examined depth- and curvature-specific between group differences in bilateral regional susceptibility (positive and negative) for each of the 34 ROIs (see Figure 2). P-values were corrected for 21 cortical depths for each ROI/curvature combination using FDR procedures.[99]

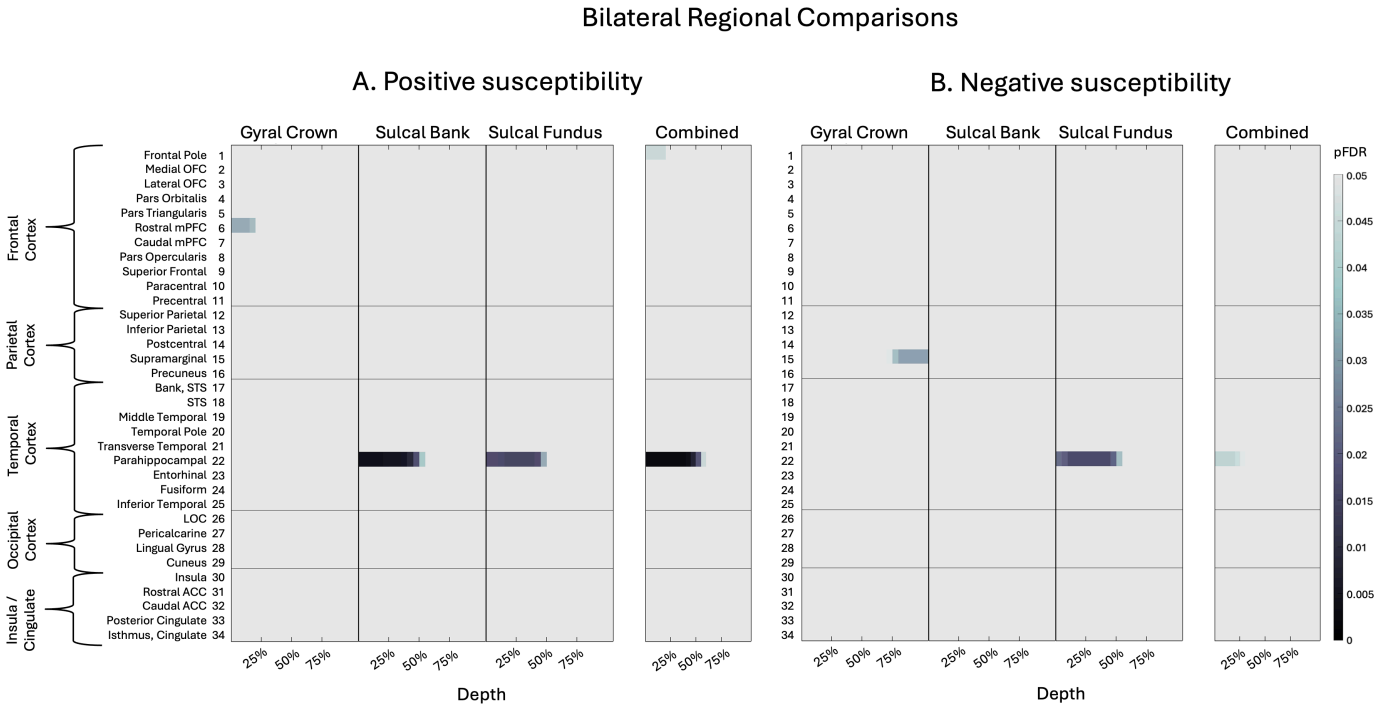

Figure 2: Bilateral regional curvature and depth results.
Colour maps demonstrate differences in magnetic susceptibility at each cortical depth (where 0% depth is proximal to the pial surface and increases toward the GM/WM boundary at 100% depth), separately for each curvature bin (crown, bank, fundus) as well as combined curvature as a whole-ROI measure. Independent sample t-tests examined group differences in susceptibility at each depth, for each curvature, at each ROI. P-values were corrected for multiple comparisons across 21 cortical depths using FDR. A. Positive susceptibility values were significantly more positive for participants with sr-mTBI than healthy controls in temporal ROIs and significantly less positive in frontal regions only. B. Susceptibility values were significantly less negative for sr-mTBI participants than controls in temporal ROIs and significantly more negative in parietal ROIs. OFC = orbitofrontal cortex; mPFC = middle prefrontal cortex; STS = superior temporal sulcus; LOC = lateral occipital cortex; ACC = anterior cingulate cortex. Figure based on Merenstein et al. (2024). Depth- and curvature-based quantitative susceptibility mapping analyses of cortical iron in Alzheimers disease. *Cerebral Cortex*.

Positive susceptibility

Across bilateral depth profiles, participants with sr-mTBI exhibited significantly higher positive susceptibility than controls in the temporal lobe only (see Figure 2A), specifically in superficial depths of the sulcal bank and fundus of the parahippocampal gyrus, a finding that was conserved when curvature was combined as a whole-ROI measure (see also Figure 3.1A and Figure 3.2A). Susceptibility was decreased following sr-mTBI in the superficial gyral crown of the rostral medial prefrontal cortex (mPFC) and superficially in the frontal pole when curvature was combined. No significant differences between groups were found in bilateral susceptibility values in parietal, occipital, or insular lobes.

Negative susceptibility

Across bilateral depth profiles, participants with sr-mTBI exhibited significantly less negative susceptibility than controls in the temporal lobe only (see Figure 2B). This finding was focal to the superficial depths of the fundus in the parahippocampal gyrus, as well as when curvature was combined (see also Figure 3.1B and Figure 3.2B). Negative susceptibility was more negative for participants with sr-mTBI deep in the supramarginal gyral crown of the parietal cortex only. No significant differences between groups for curvature were found in the sulcal bank (see Figure 3B). No significant differences were found in bilateral frontal, occipital, or insular lobes.

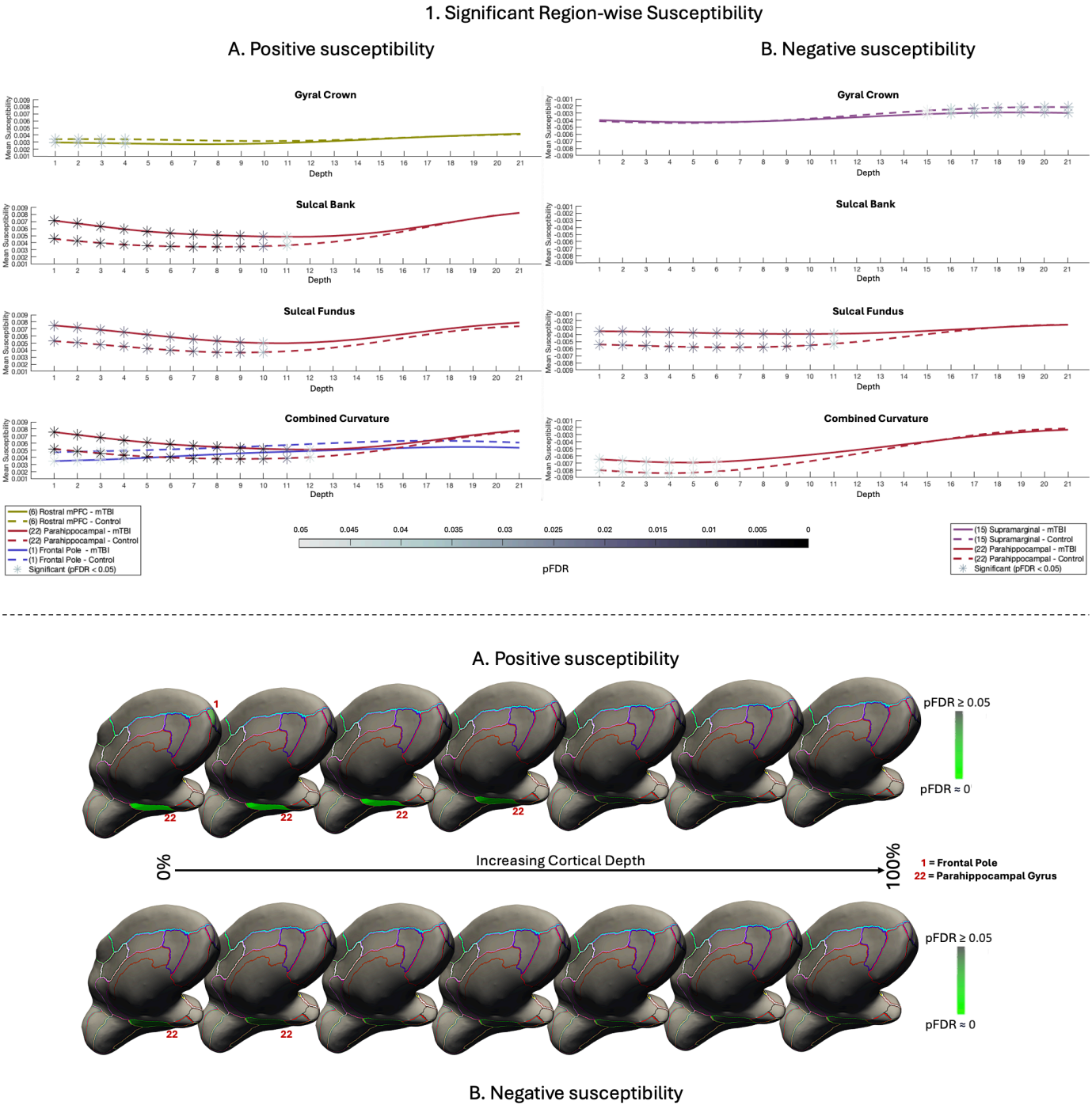

Figure 3: Significant region-wise susceptibility values.
1. Differences in susceptibility values between mTBI participants and controls for significant regions of interest only. A. Positive susceptibility values were significantly higher for participants with mTBI than healthy controls in superficial depths of the sulcal bank and fundus of the parahippocampal gyrus, as well as when curvature was combined. Values were significantly less positive for mTBI participants superficially in the gyral crown of the rostral mPFC and the superficial frontal pole when curvature was combined. B. Susceptibility values were significantly less negative for mTBI participants than controls in the superficial depths of sulcal fundus in the parahippocampal gyrus, as well as when curvature was combined. Values were significantly more negative after mTBI deep in the supramarginal gyral crown. Susceptibility is measured in parts per million (ppm). mPFC = middle prefrontal cortex. 2. Medial visualisation of significant ROIs after mTBI for both positive (A) and negative (B) susceptibility maps when curvature was combined as a whole-ROI measure. Surface lines demarcate borders between ROIs, projected onto an inflated surface. Significant ROIs are filled; intensity values relate directly to pFDR significance level. For visualisation purposes, depth was reduced from 21 to 7 by averaging pFDR values every 3 consecutive depths where 0% is proximal to the pial surface and 100% to the GM/WM interface.

Bilateral regional correlations

We used partial Pearson correlation coefficients to examine the relationship between age and regional depth-wise susceptibility (positive and negative) for combined curvature at each ROI across the entire sample, whilst controlling for group status. Additionally, we explored the correlation between susceptibility values and 1) BIST scores [70] as an indicator of injury severity, and; 2) DSI at the time of the MRI scan as a marker of injury latency, in the mTBI sample only (see Figure 4). Negative susceptibility was transformed to absolute values to better represent relationships between variables (see Figure 4B). P-values were adjusted for 21 cortical depths within each ROI using FDR methods. [99]

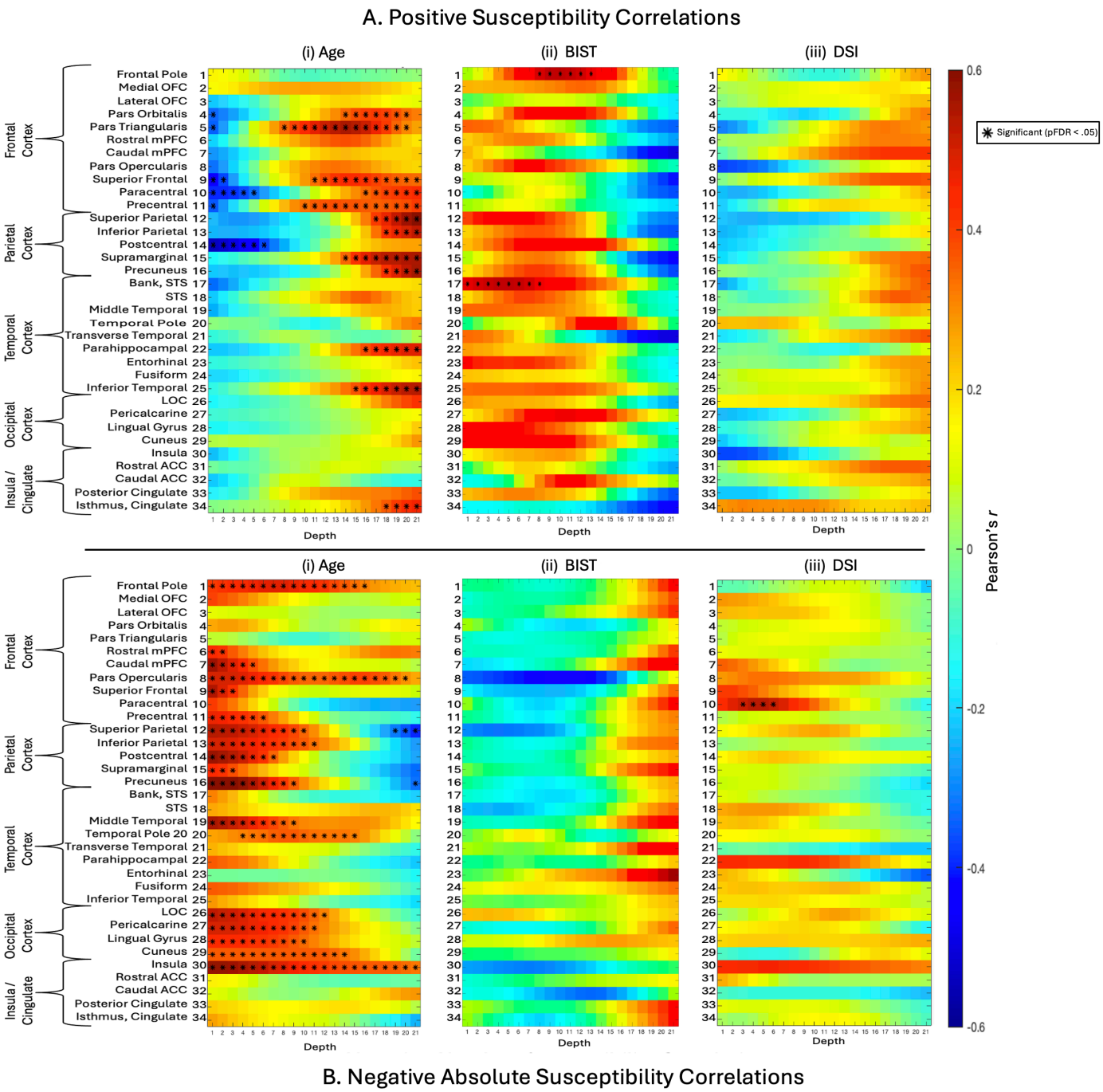

Figure 4: Correlations between positive or negative susceptibility and variables of interest
i: The relationship between age and positive (A) and negative (B) susceptibility values was assessed for each depth for combined curvature as a whole-ROI measure using partial correlations to control for the effects of group status. ii: the relationship between BIST scores as a marker for injury severity and susceptibility sign values was explored, along with; iii: the relationship between susceptibility sign values and DSI at the time of MRI scan as a marker of injury latency. Negative (B) susceptibility was transformed into absolute values to better represent the relationship between variables. BIST = Brain Injury Screening Tool; DSI = days since injury (at time of MRI scan).

Age

Positive susceptibility

We observed significant positive correlations between age and iron-related positive susceptibility distributions exclusively at deeper cortical depths near the GM/WM interface (see Figure 4A(i)). In the frontal cortex, regions with statistically significant age-related increases in positive susceptibility values included the pars orbitalis, pars triangularis, superior frontal gyrus, paracentral lobule, and precentral gyrus. In the parietal cortex, significant regions were the superior and inferior parietal lobules, supramarginal gyrus, and precuneus. In the temporal lobe, significant positive correlations were found in the parahippocampal gyrus and inferior temporal gyrus. The only cingulate region to exhibit a positive age-related correlation was the isthmus. No significant positive correlations with age were identified in any ROIs within the occipital cortex. Conversely, we identified significant negative correlations between age and positive susceptibility exclusively at superficial cortical depths near the pial surface, demonstrating an inverse pattern to the positive correlations. In the frontal cortex, the areas showing significant negative correlations were the pars orbitalis, pars triangularis, superior frontal gyrus, paracentral lobule, and precentral gyrus. In the parietal cortex, the postcentral region exhibited significant negative correlations. No significant negative correlations between positive susceptibility and age were apparent in temporal, occipital, or insular ROIs.

Negative susceptibility

Significant positive relationships were observed between absolute negative susceptibility values and age, primarily in the superficial depths of ROIs across all lobes, which at times extended to the GM/WM border (see Figure 4B(i)). In the frontal lobe, ROIs exhibiting significant positive correlations between age and negative susceptibility included the frontal pole, rostral mPFC, caudal mPFC, pars opercularis, superior frontal gyrus, and precentral gyrus. All examined ROIs in the parietal cortex exhibited significant positive relationships, namely, in the superior parietal lobule, inferior parietal lobule, postcentral gyrus, supramarginal gyrus, and precuneus. In the temporal cortex, significant positive correlations were found in the middle temporal gyrus and temporal pole. All occipital ROIs showed significant positive correlations, including the LOC, pericalcarine cortex, lingual gyrus, and cuneus. Within the insular cortex, only negative susceptibilities in the insula demonstrated a significant positive relationship with age. In contrast, significant negative correlations with age were observed only in the deeper cortical layers closer to the GM/WM junction of parietal regions, specifically in the superior parietal lobule and precuneus.

Injury severity

We observed significant positive correlations between BIST scores and positive susceptibility values in the mid-depths of the frontal pole and in superficial depths of the bank of the superior temporal sulcus (STS) (see Figure 4A(ii)). No significant correlations were observed between negative susceptibility and BIST scores (see Figure 4B(ii)).

Injury latency

No significant correlations between DSI at time of MRI and positive susceptibility values were observed for any ROI (see Figure 4A(iii)). Negative susceptibility and DSI were positively correlated in superficial depths of the bilateral paracentral gyrus in the frontal cortex only (see Figure 4B(iii)).

DISCUSSION

Previous research seeking to understand the role of brain iron following mTBI has focused primarily on susceptibility distributions in subcortical or global grey matter and/or white matter, neglecting the vulnerability of cortical regions to microstructural damage following an mTBI. The one investigation inclusive of cortical ROIs was constrained by macroscopic voxel-wise techniques, which lack the anatomical precision necessary to detect depth- or curvature-specific differences in magnetic susceptibility. To address this gap in the literature, we adapted a new analytic technique already demonstrating efficacy in Alzheimer's disease research to perform the first investigation of sr-mTBI-related differences in magnetic susceptibility as a function of cortical depth and curvature. In line with contemporary approaches in QSM research, we separated positive (iron-related) from negative (myelin-, calcium-, and protein-related) sources of susceptibility to enable more accurate estimation of underlying biological substrates.

Our findings revealed increased positive susceptibility exclusive to the temporal lobe, specifically in the superficial depths at

sulcal curvatures in the bilateral parahippocampal gyrus. This pattern was conserved when curvature was aggregated as a whole-ROI measure. In contrast, age-related positive susceptibility indicative of iron deposition was observed at deep cortical depths, closer to the interface with the white matter, in the overall sample. These findings suggest that increases in positive susceptibility close to the cortical surface indicate abnormal, injury-related iron accumulation after mTBI. Results corresponded with analyses of negative susceptibility, which demonstrated less diamagnetism in the superficial depths of the sulcal parahippocampal gyrus after mild brain trauma. In addition, negative susceptibility was positively correlated with age in superficial depths only, suggesting an alignment with age-related calcification processes in superficial cortical layers that is well supported by the literature; a pattern opposite to mTBI-related negative susceptibility effects. Fewer correlations were found between subjective injury status or time elapsed since injury and susceptibility, supporting a body of research demonstrating little relationship between objective injury measures and subjective self-report.

Depth

In-vitro histological studies have demonstrated variations in iron distribution relative to specific cortical laminae (e.g., Perls iron staining), where concentrations are lowest at the pial surface and increase progressively through GM toward its junction with WM. [100] These findings have been corroborated by iron-sensitive R_2* mapping of *ex-vivo* tissue samples using ultra-high field (7T) MRI, [100] which also exhibit high congruence with *in-vivo* QSM. [101] Taken together, these studies suggest that iron density in the cortex reflects distinct cyto- and myelo-architecture, with variance between layers. In healthy populations, iron density should be sparse at the pial surface and increase with depth. Conversely, our findings indicate an abnormal distribution pattern of positive susceptibility related to iron deposition exclusively in superficial depths of the parahippocampal gyrus in temporal cortex following injury (see Figure 2A, Figure 3.1A and Figure 3.2A). This increased positive susceptibility at the acute stage of mTBI is directly inverted for depth comparative to healthy layer-specific variation [100,101] and patterns related to normal ageing in this range of the lifespan (see Figure 4A(i)), suggesting an injury-specific model of cortical microstructural trauma (see Figure 5).

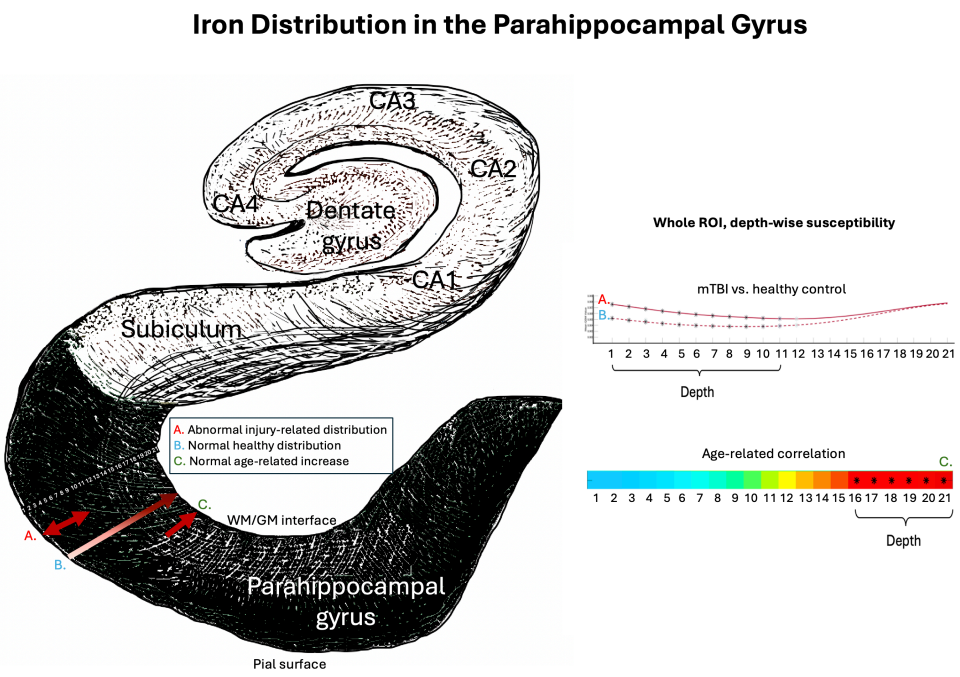

Figure 5: Iron and positive susceptibility distributions in the parahippocampal gyrus.
Visualisation of depth-specific positive (iron-related) susceptibility distributions. (A) Depicts increased positive susceptibility following mTBI relative to healthy controls restricted to superficial depths of the parahippocampal gyrus. This pattern does not overlap with (B) validated patterns of lower iron concentration proximal to the pial surface, and increasing towards the GM/WM interface as a pattern of normal layer-specific distributions, or; (C) normal age-related increases in positive susceptibility in this population (16-32 years) restricted to the deeper cortical depths closer to the GM/WM boundary. Depiction of the hippocampal formation inspired by illustration in Ranson & Clark (1959). *The anatomy of the nervous system: Its development and function* (10th ed.). W. B. Saunders Co.

The focal nature of increased positive susceptibility in superficial depths suggests iron accumulation near small blood vessels.[11] Concordantly, microhemorrhage and aggregation of activated microglia around perivascular sites are well documented after mTBI.[25,102,103] Here, it is tempting to speculate about potential mechanisms of iron overload following mTBI. Non-heme iron (i.e., bound to proteins such as ferritin and transferrin) generally enters the brain through active transport across the blood-brain-barrier (BBB) via vascular endothelial cells; a constant process that is closely regulated within the central nervous system to ensure homeostasis.[26] Injury-induced acute cerebral microvascular dysfunction and increased permeability of the BBB,[104,105] likely increases iron transport into these superficial cortical layers[22,106] which could result in a perivascular accumulation of iron. Notably, redox reactions involving non-heme iron are a significant source of reactive oxygen species (ROS);[25] when labile iron accumulates to pathological levels, it can exceed the capacity of storage proteins inducing oxidative stress, protein and DNA damage, and ferroptosis.[22,25,107] This labile iron is frequently considered a critical contributor to secondary injury mechanisms[25,26,102] and represents the primary source of paramagnetic susceptibility in the brain on QSM.[108] As such, iron accumulation acting as a catalyst for autotoxic circuits[106] is a candidate hypothesis by which iron dyshomeostasis after mTBI could account for the increased magnetic susceptibility of these compromised perivascular regions on QSM. Iron overload may represent a promising early marker of acute cell damage and mTBI-related neuropathology as well as degeneration of neural tissue downstream. However, as the precise mechanisms by which iron is released in the brain are still under investigation,[26,29] these mechanisms cannot yet be disambiguated.

Whilst the relationship between positive susceptibility and iron is well established, the mechanisms underlying diamagnetic sources of contrast are less well understood and more challenging to elucidate.[67,68,109] Recent research indicates that the primary source of diamagnetic contrast is myelin,[110] but contributions are also made by calcium[33–35] and the deposition of proteins such as amyloid-beta (Aβ).[36,37] Our results suggest that negative susceptibility is decreased in the parahippocampal gyrus at superficial depths following mTBI. Myeloarchitecture studies indicate that Layer I of cerebral cortex consists primarily of axons, dendrites, and axon terminals, the cell bodies of which are located in deeper layers.[111] Although the cerebral cortex is not well known for high myelin content,[68] decreased positive susceptibility at these superficial depths could indicate changes to surface axons. This pattern coincided with increased positive susceptibility in the superficial parahippocampal gyrus, suggesting a dual model of perivascular microstructural trauma focal to this region. The majority of iron present in the human brain parenchyma is stored as non-heme iron within myelin-maintaining oligodendroglia and in myelin itself;[112] pathological iron levels have been known to damage both.[113–115] Mechanisms leading to co-localisation of increased positive susceptibility and decreased negative susceptibility observed in this study are further supported by research into pathogenesis of multiple sclerosis, which indicates that neuroinflammation and altered BBB permeability can result in iron accumulation in macrophages and other iron-related cytotoxic events, such as oxidative stress, causing degradation of oligodendrocytes and axons.[22,113,115] Conversely, increased negative susceptibility was mostly observed at deeper cortical depths closer to the GM/WM junction, which might reflect aggregation of Aβ inherent to AD,[116] and sometimes present in CTE,[12] or calcifications known to negatively affect cognition.[117] Notably, the injury-related accumulation patterns did not overlap with age-related changes in negative susceptibility, which increased at superficial depths (see Figure 4B(i)). This suggests that both decreased negative susceptibility in superficial depths and increased negative susceptibility at deeper cortical depths may result from abnormal, injury-related, neuropathological processes.

Curvature and ROI

Prior research has noted that the sulcal fundus is particularly vulnerable to injury in mTBI due to increased susceptibility to mechanical deformation[12,64] and the 'water hammer effect.'[63] The current study supports a fundus-specific model of damage in mTBI; the only persistent differences between groups in both positive and negative susceptibility were observed in sulcal regions of the bilateral parahippocampal gyrus (positive susceptibility: sulcal bank and fundus; negative susceptibility: sulcal fundus (see Figure 2 and Figure 3)). The focal nature of injury to these concave regions extends prior work noting increased mean cortical curvature in the sulcus[118] and sulcal widening[63] after mTBI. Results are also consistent with observations of mTBI-related vascular injury and microhemorrhage in the sulcal fundus on SWI.[63] Additionally, the medial temporal lobe is a notable site of injury in sr-mTBI and previous research has highlighted the associations between sr-mTBI and loss of cortical thickness in the parahippocampal gyrus along with reductions in parahippocampal volume.[119] Contextually, the parahippocampal cortex acts as a hub region in a network

connecting areas of the frontal, parietal, and temporal lobes [120] and represents a vital link between the default-mode network and the medial temporal lobe memory system, as evidenced by resting-state fMRI studies. [121] As such, it is integral to various cognitive processes including visuospatial processing and episodic memory [122] and the facilitation of contextual associations fundamental to higher order cognitive performance. [120] The co-localisation of iron-related deposition and potential myelin changes, particularly in integrative superficial regions, within the temporal parahippocampal gyrus is consistent with the memory impairments symptomatic of sr-mTBI. [103]

Age and clinical correlates

Increasing iron in deep grey matter nuclei and some regions of the cortex is a hallmark of normal ageing. [29,60] Research indicates that age-related iron increases occur primarily in the motor and premotor cortices, as well as the superior prefrontal and parietal cortices. [60,123] Additionally, these increases have been reported in the insula [123] and hippocampus. [124] Histological evidence suggests that normal increases in cortical non-heme iron may be especially pronounced in younger individuals, sharply increasing during childhood and plateauing at around 30 years of age, depending on region. [60,125] These observations are supported by some [123,126] but not other [127] cross-sectional iron-sensitive MRI findings in adjacent age groups. Our findings support age-related cortical iron increases in a youthful population. In line with prior research, ROIs with age-related increases in likely iron content were most dense in frontal and parietal lobes, in addition to two loci in the temporal lobe and one in the insular cortex (see Figure 4A(i)). Of all cortical regions, the motor system is particularly affected by age-related iron deposition, [123] a pattern mirrored in our findings which show a notable density in the primary motor cortex. Our results suggest that age-related increases are restricted to deeper cortical depths closer to the GM/WM junction, which are known to naturally express higher iron levels in the healthy population. [100,101] These deeper layers contain large pyramidal cells, [111] which could speculatively accumulate iron differently. Indeed, previous research [67] has suggested that because age is more predictive of delayed response time rather than difficulties in decision-making, [128–130] age-related iron accumulation should show a preference for deeper layers responsible for output, rather than more integrative superficial regions. [131] In addition, we observed age-related increases in negative magnetic susceptibility exclusively close to the pial surface. Previous studies utilising negative QSM have shown similar distributions at superficial depths. [68] This pattern is well-supported in the literature, as research indicates that calcifications commonly occur in areas with high vascularization and metabolic activity, [33] such as the cortical surface. Taken together, our findings indicate that age-related increases in iron are likely restricted to deep cortical depths, while diamagnetic calcifications are likely to occur at superficial depths. Both observations are supported by strong biological plausibility and well-documented scientific evidence. This reinforces the conclusion that observed differences in both positive and negative susceptibility following sr-mTBI reflect pathological processes distinct from those associated with normal ageing.

The general lack of correlation between positive or negative susceptibilities and BIST scores may be attributed to the underreporting of symptoms notorious in sr-mTBI, [132] which would preclude accurate correlations. Whilst iron negatively correlates with cognitive symptoms in mTBI, [133] it is well-documented that subjective assessments of injury severity do not reliably reflect objective brain injury or recovery status [20] and cognitive/clinical symptoms do not align with neuroimaging findings. [21] Additionally, the lack of correlation between positive or negative susceptibilities and injury latency suggests that acute neuropathology may persist into the subacute and chronic stages, necessitating further research to elucidate the time course of secondary injury in sr-mTBI.

Implications

The role of iron in acute responses following cytotrauma, as well as its co-localisation with, and involvement in, misfolded proteins in neurodegenerative diseases, including CTE, identifies it as a potential marker of early degenerative processes. [29,30] Interestingly, the temporal lobe and hippocampus are primary loci of atrophy and tau deposition in CTE, [12,134] and iron has been found in neurofibrillary tangles within these regions. [30] In CTE, these neurofibrillary tangles favour superficial cortical layers (II/III) [135,136] and aggregate around small blood vessels, [137] especially at the sulcal fundus. [64] This laminar predilection is not seen in other tauopathies, like AD, where tau phosphorylation generally occurs in deeper layers (V/VI). [138] Indeed, this specific distribution is considered pathognomonic of CTE. [12,137] Notwithstanding the short-term effects of iron overload, which have been linked to secondary injury in mTBI, [25,102]

the association between iron-mediated oxidative stress and hyperphosphorylation of tau [27] coupled with the similarity of iron distributions observed in this study to hallmark distributions of tauopathy and degeneration in CTE raises important questions about the disease path from acute injury to eventual tissue degeneration. The precise mechanisms underlying CTE remain an active area of research, but these findings suggest that iron may serve as a candidate biomarker, warranting further investigation. Until such a time, any parallels drawn between the pattern of iron distribution in this study and the hallmark features of CTE tauopathy can, at this stage, only be speculative.

Here, follow-up investigations will be of paramount importance. A better understanding of iron and other neurobiological correlates, such as myelin damage or protein aggregation, may be essential for developing effective care and targeted treatments at the acute stage of mTBI, which could protect against adverse consequences later in life. Recent research has explored the possibility of using heavy metal chelation as a therapeutic target for iron in AD [139] and TBI. [31] In AD, this approach has had limited success, perhaps due to the accumulation of iron over a long time course; once iron overload becomes apparent, cell death has already occurred. [106] However, mechanisms of acute injury-related iron overload may be distinct from long-term aggregation. Murine models using iron chelators such as Deferoxamine [140–143] and *N*,*N*'-Di(2-hydroxybenzyl)ethylenediamine-*N*,*N*'-diacetic acid monohydrochloride (HBED) [144] have shown promise in reducing TBI symptomatology, likely through inhibition of ferroptosis and reductions in neuroinflammation, ROS, and gliosis. More research is needed to understand efficacy in humans, but this remains a possible avenue for limiting the effects of acute iron dyshomeostasis which may contribute to degenerative effects evident in later life.

Limitations and future research

While QSM offers valuable insights into iron content and distribution, at lower field strengths (i.e., 3T) voxel resolution is restricted and does not reflect specific architectonics of cortical tissue. Cortical column analyses were thus constrained to investigations of depth rather than susceptibility distribution specific to cortical laminae. Future research could benefit from applying cortical column analysis to images with higher resolutions, for example those collected on high field scanners, or by pushing images to sub-1mm resolutions insofar as signal-to-noise ratios are not compromised. The present study utilised a single-echo QSM sequence, limiting thresholding of susceptibility sources to *between* voxels. To enable thresholding *within* voxels, future studies should incorporate multi-echo sequences [101,145,146] where available, thereby enhancing the biological interpretation of the findings. Incorporating complementary modalities, such as positron emission tomography (PET), would provide a more comprehensive understanding of cellular metabolism and neurobiological processes, potentially linking these to the observed mTBI-related differences and enabling more biologically informed inferences. Inclusion of protein assays, such as blood-based biomarkers, would also aid in creating a more comprehensive picture of the biological consequences of sr-mTBI. A range of potential confounds were not controlled for in this study including prior injuries, genetic predispositions, and environmental influences, which may affect injury severity and presentation,**?** and future research should consider including additional measures to control for these variables. Given that this study was conducted exclusively in a male cohort, the generalisability of the findings to females may be limited. Sex differences in injury effects are reportedly influenced by a range of factors, including hormonal variations, [147] the use of oral contraceptives, [148] and differences in neck musculature. [149] Future research should extend investigations to female athletes and consider comparisons by sex. Finally, given the limitations of inferring long-term consequences of sr-mTBI from data collected at the acute stage, future research should prioritise longitudinal studies tracking athletes over time. This prospective approach would yield more precise information compared to retrospective studies, providing valuable insights into the relationships between the number of mTBIs sustained, iron accumulation, recovery trajectories, and long-term outcomes. In lieu of longitudinal research, planned upcoming studies will utilise comparison of individual z-scores relative to healthy population norms to better clarify the prevalence of adverse outcomes following sr-mTBI. This approach will aim to enhance our understanding of the impact of sr-mTBI at the individual level, which may be obscured by group-level analyses. [150,151]

CONCLUSIONS

To better characterise the mechanisms of mild traumatic brain injury at the acute stage, we conducted the first QSM study to assess depth- and curvature-specific regional patterns of positive (iron-related) and negative (myelin-, calcium-, and protein-related) mag-

netic susceptibility in the cerebral cortex following injury. We observed co-localisation of increased positive susceptibility with decreased negative susceptibility in the parahippocampal gyrus, indicating a possible accumulation of iron concomitant with myelin changes after injury. This distribution pattern was observed in the superficial depths of the sulcus, suggesting perivascular trauma due to mechanical forces. The pattern appeared distinct from age-related differences in positive and negative susceptibility and was reminiscent of pathognomonic patterns of tau pathology in CTE, which is known to co-localise with iron. These results support a complex, dual-pathology model of trauma after mild head injury and have implications for understanding microstructural brain tissue damage following mTBI.

AUTHOR CONTRIBUTIONS

Christi A. Essex (Conceptualization, Methodology, Project Administration, Validation, Software, Formal Analysis, Investigation, Resources, Data Curation, Writing - Original Draft, Writing - Review & Editing, Visualization); **Jenna L. Merenstein** (Methodology, Writing - Review & Editing, Visualization); **Devon K. Overson** (Methodology, Software, Visualization, Validation, Writing - Review & Editing); **Trong-Kha Truong** (Methodology, Software, Writing - Review & Editing); **David J. Madden** (Methodology, Software, Writing - Review & Editing); **Mayan J. Bedggood** (Writing - Review & Editing, Project administration, Investigation); **Helen Murray** (Writing - Review & Editing); **Samantha J. Holdsworth** (Writing - Review & Editing); **Ashley W. Stewart** (Writing - Review & Editing); **Catherine Morgan** (Writing - Review & Editing); **Richard L.M. Faull** (Writing - Review & Editing); **Patria Hume** (Writing - Review & Editing); **Alice Theadom** (Conceptualization, Methodology, Writing - Review & Editing, Funding acquisition, Supervision); **Mangor Pedersen** (Conceptualization, Methodology, Writing - Review & Editing, Funding acquisition, Supervision)

ACKNOWLEDGMENTS

We extend thanks to Amabelle Voice-Powell and Cassandra McGregor for their contribution to the data collection, and Tania Ka'ai for bringing her perspective to cultural considerations on this study. In addition, we thank Axis Sports Concussion Clinics, particularly Dr Stephen Kara, for their assistance with recruiting sr-mTBI participants and personnel at the Centre for Advanced Magnetic Resonance Imaging (CAMRI) for their assistance collecting MRI data. We also acknowledge Dr Tim Elliot for radiological reporting of all participants and Siemens Healthcare/Siemens Healthineers for the use of a work-in-progress (WIP) sequence for the acquisition of magnitude and phase images.

FUNDING

This project was funded by a grant from the Health Research Council of New Zealand (HRC), grant #21/622.

CONFLICT OF INTEREST

None to declare.

DATA AVAILABILITY

De-identified MRI data and code used for image processing and statistical analysis can be made available upon request to the corresponding author. Parent codes for cortical column generation can be made available upon request from co-authors (JLM, TKT) based at the Brain Imaging and Analysis Center at Duke University Medical Center.

REFERENCES

[1] Michael C. Dewan, Abbas Rattani, Saksham Gupta, Ronnie E. Baticulon, Ya Ching Hung, Maria Punchak, Amit Agrawal, Amos O. Adeleye, Mark G. Shrime, Andrés M. Rubiano, Jeffrey V. Rosenfeld, and Kee B. Park. Estimating the global incidence of traumatic brain injury. *Journal of Neurosurgery*, 130(4):1080–1097, 4 2019.

[2] Spencer L. James, Alice Theadom, Richard G. Ellenbogen, Marlena S. Bannick, W Cliff Montjoy-Venning, Lydia R. Lucchesi, Nooshin Abbasi, Rizwan Abdulkader, Haftom N Abraha, Jose C. Adsuar, Mohsen Afarideh, Sutapa Agrawal, Alireza Ahmadi, Muktar B. Ahmed, Amani N. Aichour, Ibtihel Aichour, Miloud T. E. Aichour, Rufus O. Akinyemi, Nadia Akseer, (...), and Christopher J. L. Murray. Global, regional, and national burden of traumatic brain injury and spinal cord injury, 1990-2016: A systematic analysis for the Global Burden of Disease Study 2016. *The Lancet Neurology*, 18(1):56–87, 1 2019.

[3] Andrew I.R. Maas, David K. Menon, Geoffrey T. Manley, Mathew Abrams, Cecilia Åkerlund, Nada Andelic, Marcel Aries, Tom Bashford, Michael J. Bell, Yelena G. Bodien, Benjamin L. Brett, András Büki, Randall M. Chesnut, Giuseppe Citerio, David Clark, Betony Clasby, Jamie D. Cooper, Endre Czeiter, Marek Czosnyka, (..), and Roger Zemek. Traumatic brain injury: progress and challenges in prevention, clinical care, and research, 11 2022.

[4] Emilie Isager Howe, Nada Andelic, Silje C.R. Fure, Cecilie Røe, Helene L. Søberg, Torgeir Hellstrøm, Øystein Spjelkavik, Heidi Enehaug, Juan Lu, Helene Ugelstad, Marianne Løvstad, and Eline Aas. Cost-effectiveness analysis of combined cognitive and vocational rehabilitation in patients with mild-to-moderate TBI: results from a randomized controlled trial. *BMC Health Services Research*, 22(1), 12 2022.

[5] Kevin M. Guskiewicz, Stephen W. Marshall, Julian Bailes, Michael Mccrea, Herndon P. Harding, Amy Matthews, Johna Register Mihalik, and Robert C. Cantu. Recurrent concussion and risk of depression in retired professional football players. *Medicine and Science in Sports and Exercise*, 39(6):903–909, 6 2007.

[6] Kerry McInnes, Christopher L. Friesen, Diane E. MacKenzie, David A. Westwood, and Shaun G. Boe. Mild Traumatic Brain Injury (mTBI) and chronic cognitive impairment: A scoping review, 4 2017.

[7] Daniel F. Mackay, Emma R. Russell, Katy Stewart, John A. MacLean, Jill P. Pell, and William Stewart. Neurodegenerative Disease Mortality among Former Professional Soccer Players. *New England Journal of Medicine*, 381(19):1801–1808, 11 2019.

[8] Kevin F. Bieniek, Melissa M. Blessing, Michael G. Heckman, Nancy N. Diehl, Amanda M. Serie, Michael A. Paolini, Bradley F. Boeve, Rodolfo Savica, R. Ross Reichard, and Dennis W. Dickson. Association between contact sports participation and chronic traumatic encephalopathy: a retrospective cohort study. *Brain Pathology*, 30(1):63–74, 1 2020.

[9] Kevin F. Bieniek, Owen A. Ross, Kerry A. Cormier, Ronald L. Walton, Alexandra Soto-Ortolaza, Amelia E. Johnston, Pamela DeSaro, Kevin B. Boylan, Neill R. Graff-Radford, Zbigniew K. Wszolek, Rosa Rademakers, Bradley F. Boeve, Ann C. McKee, and Dennis W. Dickson. Chronic traumatic encephalopathy pathology in a neurodegenerative disorders brain bank. *Acta Neuropathologica*, 130(6):877–889, 12 2015.

[10] Helen Ling, Huw R. Morris, James W. Neal, Andrew J. Lees, John Hardy, Janice L. Holton, Tamas Revesz, and David D.R. Williams. Mixed pathologies including chronic traumatic encephalopathy account for dementia in retired association football (soccer) players. *Acta Neuropathologica*, 133(3):337–352, 3 2017.

[11] Ann C. McKee, Thor D. Stein, Christopher J. Nowinski, Robert A. Stern, Daniel H. Daneshvar, Victor E. Alvarez, Hyo Soon Lee, Garth Hall, Sydney M. Wojtowicz, Christine M. Baugh, David O. Riley, Caroline A. Kubilus, Kerry A. Cormier, Matthew A. Jacobs, Brett R. Martin, Carmela R. Abraham, Tsuneya Ikezu, Robert Ross Reichard, Benjamin L. Wolozin, Andrew E. Budson, Lee E. Goldstein, Neil W. Kowall, and Robert C. Cantu. The spectrum of disease in chronic traumatic encephalopathy. *Brain*, 136(1):43–64, 2013.

[12] Ann C. McKee, Thor D. Stein, Bertrand R. Huber, John F. Crary, Kevin Bieniek, Dennis Dickson, Victor E. Alvarez, Jonathan D. Cherry, Kurt Farrell, Morgane Butler, Madeline Uretsky, Bobak Abdolmohammadi, Michael L. Alosco, Yorghos Tripodis, Jesse Mez, and Daniel H. Daneshvar. Chronic traumatic encephalopathy (CTE): criteria for neuropathological diagnosis and relationship to repetitive head impacts, 4 2023.

[13] Jesse Mez, Daniel H. Daneshvar, Patrick T. Kiernan, Bobak Abdolmohammadi, Victor E. Alvarez, Bertrand R. Huber, Michael L. Alosco, Todd M. Solomon, Christopher J. Nowinski, Lisa McHale, Kerry A. Cormier, Caroline A. Kubilus, Brett M. Martin, Lauren Murphy, Christine M. Baugh, Phillip H. Montenigro, Christine E. Chaisson, Yorghos Tripodis, Neil W. Kowall, Jennifer Weuve, Michael D. McClean, Robert C. Cantu, Lee E. Goldstein, Douglas I. Katz, Robert A. Stern, Thor D. Stein, and Ann C. McKee. Clinicopathological evaluation of chronic traumatic encephalopathy in players of American football. *JAMA - Journal of the American Medical Association*, 318(4):360–370, 7 2017.

[14] Jesse Mez, Daniel H. Daneshvar, Bobak Abdolmohammadi, Alicia S. Chua, Michael L. Alosco, Patrick T. Kiernan, Laney Evers, Laura Marshall, Brett M. Martin, Joseph N. Palmisano, Christopher J. Nowinski, Ian Mahar, Jonathan D. Cherry, Victor E. Alvarez, Brigid Dwyer, Bertrand R. Huber, Thor D. Stein, Lee E. Goldstein, Douglas I. Katz, Robert C. Cantu, Rhoda Au, Neil W. Kowall, Robert A. Stern, Michael D. McClean, Jennifer Weuve, Yorghos Tripodis, and Ann C. McKee. Duration of American Football Play and Chronic Traumatic Encephalopathy. *Annals of Neurology*, 87(1):116–131, 1 2020.

[15] Christopher C. Giza and David A. Hovda. The new neurometabolic cascade of concussion. *Neurosurgery*, 75:S24–S33, 2014.

[16] Daniel B. Hier, Tayo Obafemi-Ajayi, Matthew S. Thimgan, Gayla R. Olbricht, Sima Azizi, Blaine Allen, Bassam A. Hadi, and Donald C. Wunsch. Blood biomarkers for mild traumatic brain injury: a selective review of unresolved issues, 12 2021.

[17] Ekaterina Lunkova, Guido I. Guberman, Alain Ptito, and Rajeet Singh Saluja. Noninvasive magnetic resonance imaging techniques in mild traumatic brain injury research and diagnosis, 11 2021.

[18] Glen A. Cook and Jason S. Hawley. A review of mild traumatic brain injury diagnostics: Current perspectives, limitations, and emerging technology, 2014.

[19] Max Wintermark, Pina C. Sanelli, Yoshimi Anzai, A John Tsiouris, and Christopher T. Whitlow. Imaging evidence and recommendations for traumatic brain injury: Advanced neuro- and neurovascular imaging techniques. *American Journal of Neuroradiology*, 36(2):E1–E11, 2 2015.

[20] Michael McCrea, Timothy Meier, Daniel Huber, Alain Ptito, Erin Bigler, Chantel T. Debert, Geoff Manley, David Menon, Jen Kai Chen, Rachel Wall, Kathryn J. Schneider, and Thomas McAllister. Role of advanced neuroimaging, fluid biomarkers and genetic testing in the assessment of sport-related concussion: A systematic review, 6 2017.

[21] Martha E. Shenton, Haitham M. Hamoda, Jennifer S. Schneiderman, Sylvain Bouix, Olga Pasternak, Yogesh Rathi, M. A. Vu, Manoj P. Purohit, Karl Helmer, Inga Koerte, A Bence P. Lin, C. F. Westin, Ron Kikinis, Maciej Kubicki, Robert A. Stern, and Ross Zafonte. A review of magnetic resonance imaging and diffusion tensor imaging findings in mild traumatic brain injury, 2012.

[22] Roberta J. Ward, Fabio A. Zucca, Jeff H. Duyn, Robert R. Crichton, and Luigi Zecca. The role of iron in brain ageing and neurodegenerative disorders, 10 2014.

[23] Hongyue Ma, Yan Dong, Yanhui Chu, Yanqin Guo, and Luxin Li. The mechanisms of ferroptosis and its role in alzheimers disease, 8 2022.

[24] Elizabeth L. Mackenzie, Kenta Iwasaki, and Yoshiaki Tsuji. Intracellular iron transport and storage: From molecular mechanisms to health implications, 6 2008.

[25] Eric J. Nisenbaum, Dmitry S. Novikov, and Yvonne W. Lui. The presence and role of iron in mild traumatic brain injury: An imaging perspective. *Journal of Neurotrauma*, 31(4):301–307, 2 2014.

[26] Aleksandra Gozt, Sarah Hellewell, Phillip G.D. Ward, Michael Bynevelt, and Melinda Fitzgerald. Emerging Applications for Quantitative Susceptibility Mapping in the Detection of Traumatic Brain Injury Pathology, 7 2021.

[27] Akira Yamamoto, Ryong-Woon Shin, Kazuhiro Hasegawa, Hironobu Naiki, Hiroyuki Sato, Fumio Yoshimasu, and Tetsuyuki Kitamoto. Iron (III) induces aggregation of hyperphosphorylated s and its reduction to iron (II) reverses the aggregation: implications in the formation of neurofibrillary tangles of Alzheimer's disease. Technical report, 2002.

[28] James Stankiewicz, S Scott Panter, Mohit Neema, Ashish Arora, Courtney E Batt, and Rohit Bakshi. Iron in Chronic Brain Disorders: Imaging and Neurotherapeutic Implications. *Neurotherapeutics: The Journal of the American Society for Experimental NeuroTherapeutics*, 4:371–386, 2007.

[29] Luigi Zecca, Moussa B.H. Youdim, Peter Riederer, James R. Connor, and Robert R. Crichton. Iron, brain ageing and neurodegenerative disorders, 11 2004.

[30] Constantin Bouras, Panteleimon Giannakopoulos, Paul F. Good, Amy Hsu, Patrick R. Hof, and Daniel P. Perl. A Laser Microprobe Mass Analysis of Brain Aluminum and Iron in Dementia pugilistica: Comparison with Alzheimer's Disease. *Eur Neurol*, 38(1):53–58, 1997.

[31] Maria Daglas and Paul A. Adlard. The Involvement of Iron in Traumatic Brain Injury and Neurodegenerative Disease, 12 2018.

[32] Jeff H. Duyn and John Schenck. Contributions to magnetic susceptibility of brain tissue, 4 2017.

[33] Jinhee Jang, Yoonho Nam, Sung Won Jung, Tae Ryong Riew, Sang Hyun Kim, and In Beom Kim. Paradoxical paramagnetic calcifications in the globus pallidus: An ex vivo MR investigation and histological validation study. *NMR in Biomedicine*, 34(10), 10 2021.

[34] Sangwoo Kim, Youngjeon Lee, Chang Yeop Jeon, Keunil Kim, Youngjae Jeon, Yeung Bae Jin, Sukhoon Oh, and Chulhyun Lee. Quantitative magnetic susceptibility assessed by 7T magnetic resonance imaging in Alzheimer's disease caused by streptozotocin administration. *Quantitative Imaging in Medicine and Surgery*, 10(3):789–797, 3 2020.

[35] Yi Wang, Pascal Spincemaille, Zhe Liu, Alexey Dimov, Kofi Deh, Jianqi Li, Yan Zhang, Yihao Yao, Kelly M. Gillen, Alan H. Wilman, Ajay Gupta, Apostolos John Tsiouris, Ilhami Kovanlikaya, Gloria Chia Yi Chiang, Jonathan W. Weinsaft, Lawrence Tanenbaum, Weiwei Chen, Wenzhen Zhu, Shixin Chang, Min Lou, Brian H. Kopell, Michael G. Kaplitt, David Devos, Toshinori Hirai, Xuemei Huang, Yukunori Korogi, Alexander Shtilbans, Geon Ho Jahng, Daniel Pelletier, Susan A. Gauthier, David Pitt, Ashley I. Bush, Gary M. Brittenham, and Martin R. Prince. Clinical quantitative susceptibility mapping (QSM): Biometal imaging and its emerging roles in patient care, 10 2017.

[36] Nan Jie Gong, Russell Dibb, Marjolein Bulk, Louise van der Weerd, and Chunlei Liu. Imaging beta amyloid aggregation and iron accumulation in Alzheimer's disease using quantitative susceptibility mapping MRI. *NeuroImage*, 191:176–185, 5 2019.

[37] Zhiyong Zhao, Lei Zhang, Qingqing Wen, Wanrong Luo, Weihao Zheng, Tingting Liu, Yi Zhang, Keqing Zhu, and Dan Wu. The effect of beta-amyloid and tau protein aggregations on magnetic susceptibility of anterior hippocampal laminae in Alzheimer's diseases. *NeuroImage*, 244, 12 2021.

[38] Ferdinand Schweser, Andreas Deistung, and Jürgen R. Reichenbach. Foundations of MRI phase imaging and processing for Quantitative Susceptibility Mapping (QSM). *Zeitschrift fur Medizinische Physik*, 26(1):6–34, 3 2016.

[39] Ludovic De Rochefort, Tian Liu, Bryan Kressler, Jing Liu, Pascal Spincemaille, Vincent Lebon, Jianlin Wu, and Yi Wang. Quantitative susceptibility map reconstruction from MR phase data using bayesian regularization: Validation and application to brain imaging. *Magnetic Resonance in Medicine*, 63(1):194–206, 2010.

[40] Christian Langkammer, Kristian Bredies, Benedikt A. Poser, Markus Barth, Gernot Reishofer, Audrey Peiwen Fan, Berkin Bilgic, Franz Fazekas, Caterina Mainero, and Stefan Ropele. Fast quantitative susceptibility mapping using 3D EPI and total generalized variation. *NeuroImage*, 111:622–630, 5 2015.

[41] José P. Marques and Richard Bowtell. Application of a fourier-based method for rapid calculation of field inhomogeneity due to spatial variation of magnetic susceptibility. *Concepts in Magnetic Resonance Part B: Magnetic Resonance Engineering*, 25(1):65–78, 4 2005.

[42] Chunlei Liu, Hongjiang Wei, Nan-Jie Gong, Matthew Cronin, Russel Dibb, and Kyle Decker. Quantitative Susceptibility Mapping: Contrast Mechanisms and Clinical Applications. *Tomography*, 1(1):3–17, 9 2015.

[43] Andreas Deistung, Ferdinand Schweser, and Jürgen R. Reichenbach. Overview of quantitative susceptibility mapping, 4 2017.

[44] Chunlei Liu, Wei Li, Karen A. Tong, Kristen W. Yeom, and Samuel Kuzminski. Susceptibility-weighted imaging and quantitative susceptibility mapping in the brain, 7 2015.

[45] Sadegh Ghaderi, Sana Mohammadi, Nahid Jashire Nezhad, Shaghayegh Karami, and Fatemeh Sayehmiri. Iron quantification in basal ganglia: quantitative susceptibility mapping as a potential biomarker for Alzheimers disease a systematic review and meta-analysis, 2024.

[46] Sana Mohammadi, Sadegh Ghaderi, and Farzad Fatehi. Putamen iron quantification in diseases with neurodegeneration: a meta-analysis of the quantitative susceptibility mapping technique, 2024.

[47] Farzaneh Nikparast, Zohreh Ganji, Mohammad Danesh Doust, Reyhane Faraji, and Hoda Zare. Brain pathological changes during neurodegenerative diseases and their identification methods: How does QSM perform in detecting this process?, 12 2022.

[48] Parsa Ravanfar, Samantha M. Loi, Warda T. Syeda, Tamsyn E. Van Rheenen, Ashley I. Bush, Patricia Desmond, Vanessa L. Cropley, Darius J.R. Lane, Carlos M. Opazo, Bradford A. Moffat, Dennis Velakoulis, and Christos Pantelis. Systematic Review: Quantitative Susceptibility Mapping (QSM) of Brain Iron Profile in Neurodegenerative Diseases, 2 2021.

[49] Joseph Suresh Paul, Arun Raj T, Sheelakumari Raghavan, and Chandrasekharan Kesavadas. Comparative analysis of quantitative susceptibility mapping in preclinical dementia detection, 9 2024.

[50] Yuto Uchida, Hirohito Kan, Keita Sakurai, Kenichi Oishi, and Noriyuki Matsukawa. Quantitative susceptibility mapping as an imaging biomarker for Alzheimers disease: The expectations and limitations, 8 2022.

[51] Benjamin L. Brett, Kevin M. Koch, L. Tugan Muftuler, Matthew Budde, Michael A. Mccrea, and Timothy B. Meier. Association of Head Impact Exposure with White Matter Macrostructure and Microstructure Metrics. *Journal of Neurotrauma*, 38(4):474–484, 2 2021.

[52] Nan Jie Gong, Samuel Kuzminski, Michael Clark, Melissa Fraser, Mark Sundman, Kevin Guskiewicz, Jeffrey R. Petrella, and Chunlei Liu. Microstructural alterations of cortical and deep gray matter over a season of high school football revealed by diffusion kurtosis imaging. *Neurobiology of Disease*, 119:79–87, 11 2018.

[53] K. M. Koch, T. B. Meier, R. Karr, A. S. Nencka, L. T. Muftuler, and M. McCrea. Quantitative susceptibility mapping after sports-related concussion. *American Journal of Neuroradiology*, 39(7):1215–1221, 7 2018.

[54] Kevin M. Koch, Andrew S. Nencka, Brad Swearingen, Anne Bauer, Timothy B. Meier, and Michael McCrea. Acute Post-Concussive Assessments of Brain Tissue Magnetism Using Magnetic Resonance Imaging. *Journal of Neurotrauma*, 38(7):848–857, 4 2021.

[55] Alexander M. Weber, Anna Pukropski, Christian Kames, Michael Jarrett, Shiroy Dadachanji, Jack Taunton, David K.B. Li, and Alexander Rauscher. Pathological insights from quantitative susceptibility mapping and diffusion tensor imaging in ice hockey players pre and post-concussion. *Frontiers in Neurology*, 9(AUG), 8 2018.

[56] David K. Wright, Terence J. OBrien, and Sandy R. Shultz. Sub-acute Changes on MRI Measures of Cerebral Blood Flow and Venous Oxygen Saturation in Concussed Australian Rules Footballers. *Sports Medicine - Open*, 8(1), 12 2022.

[57] Najratun Nayem Pinky, Chantel T. Debert, Sean P. Dukelow, Brian W. Benson, Ashley D. Harris, Keith O. Yeates, Carolyn A. Emery, and Bradley G. Goodyear. Multimodal magnetic resonance imaging of youth sport-related concussion reveals acute changes in the cerebellum, basal ganglia, and corpus callosum that resolve with recovery. *Frontiers in Human Neuroscience*, 16, 10 2022.

[58] Chao Chai, Rui Guo, Chao Zuo, Linlin Fan, Saifeng Liu, Tianyi Qian, E. Mark Haacke, Shuang Xia, and Wen Shen. Decreased susceptibility of major veins in mild traumatic brain injury is correlated with post-concussive symptoms: A quantitative susceptibility mapping study. *NeuroImage: Clinical*, 15:625–632, 2017.

[59] Xuan Vinh To, Paul Cumming, and Fatima Nasrallah. From impact to recovery: tracking mild traumatic brain injury with MRIa pilot study and case series. *BMJ Open Sport & Exercise Medicine*, 10(3):e002010, 8 2024.

[60] B Hallgren and P Sourander. The effect of age on the non-haemin iron in the human brain. *Journal of Neurochemistry*, 3:41–51, 1958.

[61] Mark E. Haacke, Norman Y.C. Cheng, Michael J. House, Qiang Liu, Jaladhar Neelavalli, Robert J. Ogg, Asadullah Khan, Muhammad Ayaz, Wolff Kirsch, and Andre Obenaus. Imaging iron stores in the brain using magnetic resonance imaging. *Magnetic Resonance Imaging*, 23(1):1–25, 2005.

[62] Eytan Raz, Jens H. Jensen, Yulin Ge, James S. Babb, L. Miles, Joesph Reaume, Robert I. Grossman, and Matilde Inglese. Brain iron quantification in mild traumatic brain injury: A magnetic field correlation study. *American Journal of Neuroradiology*, 32(10):1851–1856, 11 2011.

[63] Steven Kornguth, Neal Rutledge, Gabe Perlaza, James Bray, and Allen Hardin. A Proposed Mechanism for Development of CTE Following Concussive Events: Head Impact, Water Hammer Injury, Neurofilament Release, and Autoimmune Processes. *Brain Sciences*, 7(12):164, 2017.

[64] Douglas H. Smith, Victoria E. Johnson, and William Stewart. Chronic neuropathologies of single and repetitive TBI: Substrates of dementia? *Nature Reviews Neurology*, 9(4):211–221, 4 2013.

[65] Miriam D. Waehnert, Juliane Dinse, Andreas Schäfer, Stefan Geyer, Pierre Louis Bazin, Robert Turner, and Christine Lucas Tardif. A subject-specific framework for in vivo myeloarchitectonic analysis using high resolution quantitative MRI. *NeuroImage*, 125:94–107, 1 2016.

[66] Yixin Ma, Iain P. Bruce, Chun Hung Yeh, Jeffrey R. Petrella, Allen W. Song, and Trong Kha Truong. Column-based cortical depth analysis of the diffusion anisotropy and radiality in submillimeter whole-brain diffusion tensor imaging of the human cortical gray matter in vivo. *NeuroImage*, 270, 4 2023.

[67] Jenna L. Merenstein, Jiayi Zhao, Devon K. Overson, Trong Kha Truong, Kim G. Johnson, Allen W. Song, and David J. Madden. Depth- and curvature-based quantitative susceptibility mapping analyses of cortical iron in Alzheimers disease. *Cerebral Cortex*, 34(2), 2 2024.

[68] Alicia Northall, Juliane Doehler, Miriam Weber, Stefan Vielhaber, Stefanie Schreiber, and Esther Kuehn. Layer-specific vulnerability is a mechanism of topographic map aging. *Neurobiology of Aging*, 128:17–32, 8 2023.

[69] Miriam D. Waehnert, Juliane Dinse, Marcel Weiss, Markus N. Streicher, P. Waehnert, Stefan Geyer, Robert Turner, and Pierre-Louis Bazin. Anatomically motivated modeling of cortical laminae. *NeuroImage*, 93:210–220, 6 2014.

[70] Alice Theadom, Natalie Hardaker, Charlotte Bray, Richard Siegert, Kevin Henshall, Katherine Forch, Kris Fernando, Doug King, Mark Fulcher, Sam Jewell, Nusratnaaz Shaikh, Renata Bastos Gottgtroy, and Patria Hume. The Brain Injury Screening Tool (BIST): Tool development, factor structure and validity. *PLoS ONE*, 16(2 February), 2 2021.

[71] Krzysztof J. Gorgolewski, Tibor Auer, Vince D. Calhoun, R. Cameron Craddock, Samir Das, Eugene P. Duff, Guillaume Flandin, Satrajit S. Ghosh, Tristan Glatard, Yaroslav O. Halchenko, Daniel A. Handwerker, Michael Hanke, David Keator, Xiangrui Li, Zachary Michael, Camille Maumet, B. Nolan Nichols, Thomas E. Nichols, John Pellman, Jean Baptiste Poline, Ariel Rokem, Gunnar Schaefer, Vanessa Sochat, William Triplett, Jessica A. Turner, Gaël Varoquaux, and Russell A. Poldrack. The brain imaging data structure, a format for organizing and describing outputs of neuroimaging experiments. *Scientific Data*, 3, 6 2016.

[72] Arnaud Boré, Samuel Guay, Christophe Bedetti, Steven Meisler, and Nick GuenTher. Dcm2Bids, August 2023.

[73] Xiangrui Li, Paul S. Morgan, John Ashburner, Jolinda Smith, and Christopher Rorden. The first step for neuroimaging data analysis: DICOM to NIfTI conversion. *Journal of Neuroscience Methods*, 264:47–56, 5 2016.

[74] Nicholas J. Tustison, Brian B. Avants, Philip A. Cook, Yuanjie Zheng, Alexander Egan, Paul A. Yushkevich, and James C. Gee. N4ITK: Improved N3 bias correction. *IEEE Transactions on Medical Imaging*, 29(6):1310–1320, 6 2010.

[75] Brian B. Avants, Nicholas J. Tustison, Gang Song, Philip A. Cook, Arno Klein, and James C. Gee. A reproducible evaluation of ANTs similarity metric performance in brain image registration. *NeuroImage*, 54(3):2033–2044, 2 2011.

[76] Bruce Fischl. FreeSurfer, 8 2012.

[77] Ashley W. Stewart and Stefan. Bollman. QSMxT/QSMxT, 2022.

[78] Angela I. Renton, Thuy T. Dao, Tom Johnstone, Oren Civier, Ryan P. Sullivan, David J. White, Paris Lyons, Benjamin M. Slade, David F. Abbott, Toluwani J. Amos, Saskia Bollmann, Andy Botting, Megan E.J. Campbell, Jeryn Chang, Thomas G. Close, Monika Dörig, Korbinian Eckstein, Gary F. Egan, Stefanie Evas, Guillaume Flandin, Kelly G. Garner, Marta I. Garrido, Satrajit S. Ghosh, Martin Grignard, Yaroslav O. Halchenko, Anthony J. Hannan, Anibal S. Heinsfeld, Laurentius Huber, Matthew E. Hughes, Jakub R. Kaczmarzyk, Lars Kasper, Levin Kuhlmann, Kexin Lou, Yorguin Jose Mantilla-Ramos, Jason B. Mattingley, Michael L. Meier, Jo Morris, Akshaiy Narayanan, Franco Pestilli, Aina Puce, Fernanda L. Ribeiro, Nigel C. Rogasch, Chris Rorden, Mark M. Schira, Thomas B. Shaw, Paul F. Sowman, Gershon Spitz, Ashley W. Stewart, Xincheng Ye, Judy D. Zhu, Aswin Narayanan, and Steffen Bollmann. Neurodesk: an accessible, flexible and portable data analysis environment for reproducible neuroimaging. *Nature Methods*, 2024.

[79] Barbara Dymerska, Korbinian Eckstein, Beata Bachrata, Bernard Siow, Siegfried Trattnig, Karin Shmueli, and Simon Daniel Robinson. Phase unwrapping with a rapid opensource minimum spanning tree algorithm (ROMEO). *Magnetic Resonance in Medicine*, 85(4):2294–2308, 4 2021.

[80] Tian Liu, Ildar Khalidov, Ludovic de Rochefort, Pascal Spincemaille, Jing Liu, A. John Tsiouris, and Yi Wang. A novel background field removal method for MRI using projection onto dipole fields (PDF). *NMR in Biomedicine*, 24(9):1129–1136, 11 2011.

[81] Christian Kames, Vanessa Wiggermann, and Alexander Rauscher. Rapid two-step dipole inversion for susceptibility mapping with sparsity priors. *NeuroImage*, 167:276–283, 2 2018.

[82] Berkin Bilgic, Mauro Costagli, Kwok-Shing Chan, Jeff Duyn, Christian Langkammer, Jongho Lee, Xu Li, Chunlei Liu, José P Marques, Carlos Milovic, Simon Robinson, Ferdinand Schweser, Karin Shmueli, Pascal Spincemaille, Sina Straub, Peter Van Zijl, and Yi Wang. Recommended Implementation of Quantitative Susceptibility Mapping for Clinical Research in The Brain: A Consensus of the ISMRM Electro-Magnetic Tissue Properties Study Group. Technical report, 2023.

[83] Ashley W. Stewart, Simon D. Robinson, Kieran OBrien, Jin Jin, Georg Widhalm, Gilbert Hangel, Angela Walls, Jonathan Goodwin, Korbinian Eckstein, Monique Tourell, Catherine Morgan, Aswin Narayanan, Markus Barth, and Steffen Bollmann. QSMxT: Robust masking and artifact reduction for quantitative susceptibility mapping. *Magnetic Resonance in Medicine*, 87(3):1289–1300, 3 2022.

[84] Stephen M. Smith. Fast robust automated brain extraction. *Human Brain Mapping*, 17(3):143–155, 11 2002.

[85] Nobuyuki Otsu. A Threshold Selection Method from Gray-level Histograms (OTSU). *IEEE Transactions on Systems, Man, and Cybernetics*, SMC-9(1), 1979.

[86] Mark Jenkinson, Christian F. Beckmann, Timothy E.J. Behrens, Mark W. Woolrich, and Stephen M. Smith. FSL. *NeuroImage*, 62(2):782–790, 8 2012.

[87] Stephen M. Smith, Mark Jenkinson, Mark W. Woolrich, Christian F. Beckmann, Timothy E.J. Behrens, Heidi Johansen-Berg, Peter R. Bannister, Marilena De Luca, Ivana Drobnjak, David E. Flitney, Rami K. Niazy, James Saunders, John Vickers, Yongyue Zhang, Nicola De Stefano, J. Michael Brady, and Paul M. Matthews. Advances in functional and structural MR image analysis and implementation as FSL. In *NeuroImage*, volume 23, 2004.

[88] Mark W. Woolrich, Saad Jbabdi, Brian Patenaude, Michael Chappell, Salima Makni, Timothy Behrens, Christian Beckmann, Mark Jenkinson, and Stephen M. Smith. Bayesian analysis of neuroimaging data in FSL. *NeuroImage*, 45(1 Suppl), 2009.

[89] Douglas N. Greve and Bruce Fischl. Accurate and robust brain image alignment using boundary-based registration. *NeuroImage*, 48(1):63–72, 10 2009.

[90] Mark Jenkinson, Peter Bannister, Michael Brady, and Stephen Smith. Improved Optimization for the Robust and Accurate Linear Registration and Motion Correction of Brain Images. *NeuroImage*, 17(2):825–841, 10 2002.

[91] Mark Jenkinson and Stephen Smith. A global optimisation method for robust affine registration of brain images. Technical report, 2001.

[92] Jürgen R. Reichenbach. The future of susceptibility contrast for assessment of anatomy and function, 8 2012.

[93] Alessandro Daducci, Stephan Gerhard, Alessandra Griffa, Alia Lemkaddem, Leila Cammoun, Xavier Gigandet, Reto Meuli, Patric Hagmann, and Jean Philippe Thiran. The Connectome Mapper: An Open-Source Processing Pipeline to Map Connectomes with MRI. *PLoS ONE*, 7(12), 12 2012.

[94] Leila Cammoun, Xavier Gigandet, Djalel Meskaldji, Jean Philippe Thiran, Olaf Sporns, Kim Q. Do, Philippe Maeder, Reto Meuli, and Patric Hagmann. Mapping the human connectome at multiple scales with diffusion spectrum MRI. *Journal of Neuroscience Methods*, 203(2):386–397, 1 2012.

[95] Rahul S. Desikan, Florent Ségonne, Bruce Fischl, Brian T. Quinn, Bradford C. Dickerson, Deborah Blacker, Randy L. Buckner, Anders M. Dale, R. Paul Maguire, Bradley T. Hyman, Marilyn S. Albert, and Ronald J. Killiany. An automated labeling system for subdividing the human cerebral cortex on MRI scans into gyral based regions of interest. *NeuroImage*, 31(3):968–980, 7 2006.

[96] Donald J. Tournier, Robert Smith, David Raffelt, Rami Tabbara, Thijs Dhollander, Maximilian Pietsch, Daan Christiaens, Ben Jeurissen, Chun Hung Yeh, and Alan Connelly. MRtrix3: A fast, flexible and open software framework for medical image processing and visualisation, 11 2019.

[97] Rudolph Pienaar, Bruce Fischl, Verne Caviness, N Makris, and Patricia E Grant. A Methodology for analyzing curvature in the developing brain from preterm to adult. *International Journal of Imaging Systems and Technology*, 18(1), 2008.

[98] Bruce Fischl, Anders M Dale, and Marcus E Raichle. Measuring the thickness of the human cerebral cortex from magnetic resonance images. *PNAS*, 97(20):11050–11055, 2000.

[99] Yoav Benjamini and Yosef Hochberg. Controlling the False Discovery Rate: A Practical and Powerful Approach to Multiple. Technical Report 1, 1995.

[100] Masaki Fukunaga, Tie Qiang Li, Peter Van Gelderen, Jacco A. De Zwart, Karin Shmueli, Bing Yao, Jongho Lee, Dragan Maric, Maria A. Aronova, Guofeng Zhang, Richard D. Leapman, John F. Schenck, Hellmut Merkle, and Jeff H. Duyn. Layer-specific variation of iron content in cerebral cortex as a source of MRI contrast. *Proceedings of the National Academy of Sciences of the United States of America*, 107(8):3834–3839, 2 2010.

[101] Jingu Lee, Young Hyun Yun, Seong Ho Yoo, Jinhee Jang, Hong Oh, Yoonho Nam, Sehoon Jung, Sunhye Kim, Masaki Fukunaga, Woojun Kim, Hyung Jin Choi, and Jongho Lee. In-vivo histology of iron and myelin in the brain using magnetic susceptibility source separation in MRI.

[102] Suna Huang, Su Li, Hua Feng, and Yujie Chen. Iron Metabolism Disorders for Cognitive Dysfunction After Mild Traumatic Brain Injury, 3 2021.

[103] Ann C. Mckee and Daniel H. Daneshvar. The neuropathology of traumatic brain injury. In *Handbook of Clinical Neurology*, volume 127, pages 45–66. Elsevier B.V., 2015.

[104] Danielle K. Sandsmark, Asma Bashir, Cheryl L. Wellington, and R. Diaz-Arrastia. Cerebral Microvascular Injury: A Potentially Treatable Endophenotype of Traumatic Brain Injury-Induced Neurodegeneration, 8 2019.

[105] Yingxi Wu, Haijian Wu, Xinying Guo, Brock Pluimer, and Zhen Zhao. BloodBrain Barrier Dysfunction in Mild Traumatic Brain Injury: Evidence From Preclinical Murine Models, 8 2020.

[106] Sonia Levi, Maddalena Ripamonti, Andrea Stefano Moro, and Anna Cozzi. Iron imbalance in neurodegeneration, 4 2024.

[107] Marcin Kruszewski. Labile iron pool: The main determinant of cellular response to oxidative stress. In *Mutation Research - Fundamental and Molecular Mechanisms of Mutagenesis*, volume 531, pages 81–92. Elsevier, 10 2003.

[108] Christian Langkammer, Ferdinand Schweser, Nikolaus Krebs, Andreas Deistung, Walter Goessler, Eva Scheurer, Karsten Sommer, Gernot Reishofer, Kathrin Yen, Franz Fazekas, Stefan Ropele, and Jürgen R. Reichenbach. Quantitative susceptibility mapping (QSM) as a means to measure brain iron? A post mortem validation study. *NeuroImage*, 62(3):1593–1599, 9 2012.

[109] David J. Madden and Jenna L. Merenstein. Quantitative susceptibility mapping of brain iron in healthy aging and cognition. *NeuroImage*, 282, 11 2023.

[110] Kofi Deh, Gerald D. Ponath, Zaki Molvi, Gian Carlo T. Parel, Kelly M. Gillen, Shun Zhang, Thanh D. Nguyen, Pascal Spincemaille, Yinghua Ma, Ajay Gupta, Susan A. Gauthier, David Pitt, and Yi Wang. Magnetic susceptibility increases as diamagnetic molecules breakdown: Myelin digestion during multiple sclerosis lesion formation contributes to increase on QSM. *Journal of Magnetic Resonance Imaging*, 48(5):1281–1287, 11 2018.

[111] Yasushi Miyashita. Operating principles of the cerebral cortex as a six-layered network in primates: beyond the classic canonical circuit model. *Proceedings of the Japan Academy Series B: Physical and Biological Sciences*, 98(3):93–111, 2022.

[112] James R Connor and Sharon L Menzies. Cellular management of iron in the brain. Technical report, 1995.

[113] Monika Bradl and Hans Lassmann. Oligodendrocytes: Biology and pathology, 1 2010.

[114] Simon Hametner, Isabella Wimmer, Lukas Haider, Sabine Pfeifenbring, Wolfgang Brück, and Hans Lassmann. Iron and neurodegeneration in the multiple sclerosis brain. *Annals of Neurology*, 74(6):848–861, 12 2013.

[115] Hans Lassmann, Jack Van Horssen, and Don Mahad. Progressive multiple sclerosis: Pathology and pathogenesis, 2012.

[116] H Braak and E Braak. Neuropathological stageing of Alzheimer-related changes. *Acta Neuropathol*, 82:239–259, 1991.

[117] Olivier Thibault, John C. Gant, and Philip W. Landfield. Expansion of the calcium hypothesis of brain aging and Alzheimer's disease: Minding the store, 6 2007.

[118] Jace B. King, Melissa P. Lopez-Larson, and Deborah A. Yurgelun-Todd. Mean cortical curvature reflects cytoarchitecture restructuring in mild traumatic brain injury. *NeuroImage: Clinical*, 11:81–89, 2016.

[119] Hector Arciniega, Zachary H Baucom, Fatima Tuz-Zahra, Yorghos Tripodis, Holly Carrington, Nicholas Kim, Evdokiya E Knyazhanskaya, Leonard B Jung, Katherine Breedlove, Tim L T Wiegand, Daniel H Daneshvar, R Jarrett Rushmore, Tashrif Billah, Ofer Pasternak, Michael J Coleman, and Charles H Adler. Brain morphometry in former American football players: 1 findings from the DIAGNOSE CTE research project. *Oxford University Press*, 22, 2024.

[120] Flavius D. Raslau, Ian T. Mark, A. P. Klein, John L. Ulmer, Vikram Mathews, and Leighton P. Mark. Memory Part 2: The Role of the Medial Temporal Lobe. *American Journal of Neuroradiology*, 36(5):846–849, 5 2015.

[121] Andrew M. Ward, Aaron P. Schultz, Willem Huijbers, Koene R.A. Van Dijk, Trey Hedden, and Reisa A. Sperling. The parahippocampal gyrus links the default-mode cortical network with the medial temporal lobe memory system. *Human Brain Mapping*, 35(3):1061–1073, 3 2014.

[122] Elissa M. Aminoff, Kestutis Kveraga, and Moshe Bar. The role of the parahippocampal cortex in cognition, 8 2013.

[123] Julio Acosta-Cabronero, Matthew J. Betts, Arturo Cardenas-Blanco, Shan Yang, and Peter J. Nestor. In vivo MRI mapping of brain iron deposition across the adult lifespan. *Journal of Neuroscience*, 36(2):364–374, 1 2016.

[124] Jesper Hagemeier, Jeroen J.G. Geurts, and Robert Zivadinov. Brain iron accumulation in aging and neurodegenerative disorders, 12 2012.

[125] John F. Schenck and Earl A. Zimmerman. High-field magnetic resonance imaging of brain iron: Birth of a biomarker?, 11 2004.

[126] Martina F. Callaghan, Patrick Freund, Bogdan Draganski, Elaine Anderson, Marinella Cappelletti, Rumana Chowdhury, Joern Diedrichsen, Thomas H.B. FitzGerald, Peter Smittenaar, Gunther Helms, Antoine Lutti, and Nikolaus Weiskopf. Widespread age-related differences in the human brain microstructure revealed by quantitative magnetic resonance imaging. *Neurobiology of Aging*, 35(8):1862–1872, 2014.

[127] Karen M. Rodrigue, E. Mark Haacke, and Naftali Raz. Differential effects of age and history of hypertension on regional brain volumes and iron. *NeuroImage*, 54(2):750–759, 1 2011.

[128] Roger Ratcliff. Modeling Aging Effects on Two-Choice Tasks: Response Signal and Response Time Data. *Psychology and Aging*, 23(4):900–916, 12 2008.

[129] David J. Madden, Rachel E. Siciliano, Catherine W. Tallman, Zachary A. Monge, Andreas Voss, and Jessica R. Cohen. Response-level processing during visual feature search: Effects of frontoparietal activation and adult age. *Attention, Perception, and Psychophysics*, 82(1):330–349, 1 2020.

[130] Jenna L. Merenstein, Hollie A. Mullin, and David J. Madden. Age-related differences in frontoparietal activation for target and distractor singletons during visual search. *Attention, Perception, and Psychophysics*, 85(3):749–768, 4 2023.

[131] Edmund T. Rolls and W. Patrick C. Mills. Computations in the deep vs superficial layers of the cerebral cortex. *Neurobiology of Learning and Memory*, 145:205–221, 11 2017.

[132] Timothy B. Meier, Bradley J. Brummel, Rashmi Singh, Christopher J. Nerio, David W. Polanski, and Patrick S.F. Bellgowan. The underreporting of self-reported symptoms following sports-related concussion. *Journal of Science and Medicine in Sport*, 18(5):507–511, 9 2015.

[133] Liyan Lu, Heli Cao, Xiaoer Wei, Yuehua Li, and Wenbin Li. Iron Deposition Is Positively Related to Cognitive Impairment in Patients with Chronic Mild Traumatic Brain Injury: Assessment with Susceptibility Weighted Imaging. *BioMed Research International*, 2015, 2015.

[134] Helen C. Murray, Chelsie Osterman, Paige Bell, Luca Vinnell, and Maurice A. Curtis. Neuropathology in chronic traumatic encephalopathy: a systematic review of comparative post-mortem histology literature, 12 2022.

[135] Alan J. Pearce, Joanne Sy, Maggie Lee, Antony Harding, Rowena Mobbs, Jennifer Batchelor, Catherine M. Suter, and Michael E. Buckland. Chronic traumatic encephalopathy in a former Australian rules football player diagnosed with Alzheimer's disease, 2 2020.

[136] T Tokuda, S Lkeda, N Yanagisawa, Y Lhara, and G G Glenner. Am Nii6pathologica Re-examination of ex-boxers' brains using immunohistochemistry with antibodies to amyloid [-protein and tau protein*. Technical report, 1991.

[137] Ann C. McKee, Nigel J. Cairns, Dennis W. Dickson, Rebecca D. Folkerth, C. Dirk Keene, Irene Litvan, Daniel P. Perl, Thor D. Stein, Jean Paul Vonsattel, William Stewart, Yorghos Tripodis, John F. Crary, Kevin F. Bieniek, Kristen Dams-OConnor, Victor E. Alvarez, and Wayne A. Gordon. The first NINDS/NIBIB consensus meeting to define neuropathological criteria for the diagnosis of chronic traumatic encephalopathy. *Acta Neuropathologica*, 131(1):75–86, 1 2016.

[138] R C A Pearson, M M Esirit, R W Hiornst, G K Wilcock, and T P S Powell. Anatomical correlates of the distribution of the pathological changes in the neocortex in Alzheimer disease (neurofibrillary tangles/lamination/clustering). Technical report, 1985.

[139] Tomasz Mazur, Magdalena Malik, and Dariusz C. Bieńko. The impact of chelating compounds on Cu2+, Fe2+/3+, and Zn2+ ions in Alzheimer's disease treatment, 8 2024.

[140] Haoran Jia, Xilei Liu, Yiyao Cao, Hanhong Niu, Lan Zhang, Rui Jun Li, Fanjian Li, Dongdong Sun, Mingming Shi, Liang Wa, Xiao Liu, Guili Yang, Fanglian Chen, Shu Zhang, and Jianning Zhang. Deferoxamine ameliorates neurological dysfunction by inhibiting ferroptosis and neuroinflammation after traumatic brain injury. *Brain Research*, 1812, 8 2023.

[141] Dorothy A Long, Kamalika Ghosh, Anthony N Moore, C Edward Dixon, and Pramod K Dash. Deferoxamine improves spatial memory performance following experimental brain injury in rats. Technical report, 1996.

[142] S Scott Panter, J Mark Braughler, and Edward D Hall. Dextran-Coupled Deferoxamine Improves Outcome in a Murine Model of Head Injury. *Journal of Neurotrauma*, 9(1), 1992.

[143] Jinbing Zhao, Zhi Chen, Guohua Xi, Richard F. Keep, and Ya Hua. Deferoxamine Attenuates Acute Hydrocephalus After Traumatic Brain Injury in Rats. *Translational Stroke Research*, 5(5):586–594, 2014.

[144] Saher Khalaf, Abdullah Shafique Ahmad, K. V.D.Ranga Chamara, and Sylvain Doré. Unique Properties Associated with the Brain Penetrant Iron Chelator HBED Reveal Remarkable Beneficial Effects after Brain Trauma. *Journal of Neurotrauma*, 36(1):43–53, 1 2019.

[145] Subin Lee, Hyeong Geol Shin, Minjun Kim, and Jongho Lee. Depth-wise profiles of iron and myelin in the cortex and white matter using χ-separation: A preliminary study. *NeuroImage*, 273, 6 2023.

[146] Zhenghao Li, Ruimin Feng, Qiangqiang Liu, Jie Feng, Guoyan Lao, Ming Zhang, Jun Li, Yuyao Zhang, and Hongjiang Wei. APART-QSM: An improved sub-voxel quantitative susceptibility mapping for susceptibility source separation using an iterative data fitting method. *NeuroImage*, 274, 7 2023.

[147] Kathryn Wunderle, Kathleen M. Hoeger, Erin Wasserman, and Jeffrey J. Bazarian. Menstrual phase as predictor of outcome after mild traumatic brain injury in women. *Journal of Head Trauma Rehabilitation*, 29(5):E1–E8, 9 2014.

[148] Virginia Gallagher, Natalie Kramer, Kristin Abbott, John Alexander, Hans Breiter, Amy Herrold, Tory Lindley, Jeffrey Mjaanes, and James Reilly. The effects of sex differences and hormonal contraception on outcomes after collegiate sports-related concussion. *Journal of Neurotrauma*, 35(11):1242–1247, 6 2018.

[149] Ryan T. Tierney, Michael R. Sitler, C. Buz Swanik, Kathleen A. Swanik, Michael Higgins, and Joseph Torg. Gender differences in head-neck segmnet dynamic stabilization during head accelaration. *Medicine and Science in Sports and Exercise*, 37(2):272–279, 2 2005.

[150] Mayan J. Bedggood, Christi A. Essex, Alice Theadom, Samantha J. Holdsworth, Richard L.M. Faull, and Mangor Pedersen. Individual-level analysis of MRI T2 relaxometry in mild traumatic brain injury: Possible indications of brain inflammation. *NeuroImage: Clinical*, 43, 1 2024.

[151] Juan F. Domínguez D, Ashley Stewart, Alex Burmester, Hamed Akhlaghi, Kieran O'Brien, Steffen Bollmann, and Karen Caeyenberghs. Improving quantitative susceptibility mapping for the identification of traumatic brain injury neurodegeneration at the individual level. *Zeitschrift fur Medizinische Physik*, 2024.